Implications of Tectonic Anomalies From Potential Field Data in Some Parts of Southeast Nigeria.

STEPHEN EGUBA EKWOK (styvneguba@yahoo.com)
UNIVERSITY OF CALABAR, CALABAR https://orcid.org/0000-0002-5170-9648
Anthony Effiong Akpan
University of Calabar
Ogiji-Idaga Martins Achadu
university of calabar
Christian Atelwhobel Ulem
University of Calabar

Research Article

Keywords: Magnetic method, Gravity method, Magmatic intrusion, Mineralization, Lower Benue Trough, Southeast Nigeria.

Posted Date: March 18th, 2021

DOI: https://doi.org/10.21203/rs.3.rs-310002/v1

Version of Record: A version of this preprint was published at Environmental Earth Sciences on December 6th, 2021. See the published version at https://doi.org/10.1007/s12665-021-10060-7.

Implications of tectonic anomalies from potential field data in some parts of Southeast Nigeria.

[1]Stephen E. Ekwok*, [1]Anthony E. Akpan, [2]Ogiji-Idaga M. Achadu and

[1]Christian A. Ulem

1. Applied Geophysics Programme, Department of Physics, University of Calabar, PMB 1115, Calabar, Cross River State, Nigeria

2. Department of Geology, University of Calabar, PMB 1115, Calabar, Cross River State, Nigeria

Corresponding author: styvneguba@yohoo.com

Phone number: +2348034693380

Abstract

Tectonic structures controlling mineralization in some parts of Southeast Nigeria were evaluated using airborne potential field data**.** High and low frequency filters and depth determination tools were adopted to evaluate short and long wavelength anomalies, resolve the spatial spreading of igneous intrusions, depths to geologic sources and basin topography. The high frequency results exhibited high concentration of short wavelength anomalies in the Obudu Plateau and Ikom-Mamfe Rift. The underlying main tectonics of the area elucidated by the low frequency results caused the widespread occurrences of short wavelength geologic structures that are revealed by the high frequency maps. The study area is characterized by comparatively thin (~13.0 to <3000 m) sedimentation. The observed thin thickness is as a result of the massive Precambrian basement outcrops in some locations in the Obudu Plateau and the proliferation of igneous intrusions within this part of the Lower Benue Trough. The 2-D models showed the undulating nature of the underlying basin topography, the location of intrusions, domal structures and related normal faults. The locations and neighbourhood of intrusions and/or short wavelength structures are viable sites for lead-zinc-barite, brine and metallogenic minerals.

Keyword: Magnetic method; Gravity method; Magmatic intrusion; Mineralization; Lower Benue Trough; Southeast Nigeria.

HIGHLIGHTS

- Lineaments serve as potential pathway for hydrothermal fluid migration and mineralization
- The deeply buried long wavelength anomalies caused the surficial short wavelength anomalies
- Zones of intrusions and short wavelength anomalies are possible areas of mineralization.

1.0 Introduction

The evolution of the Nigerian Basement Complexes and Benue Trough were considered in the light of tectonothermal and global tectonic events respectively (Agbi and Ekwueme, 2018; Burke and Dewey, 1974). Over time, geologic structures in the Precambrian basement rocks were caused by the intrusions of Mesozoic calc alkaline ring complexes that is, younger granites (Woakes *et al.,* 1987). Similarly, the Cretaceous Lower Benue Trough (LBT) was vastly invaded by basic and intermediate intrusives of the Santonian Abakaliki Anticlinorium and Quaternary-Recent Cameroon Volcanic Line (Ekwok *et al.,* 2019; Benkhelil, 1987). These happenings resulted to the development of various geologic structures, chemical processes and hydrothermal variations of the host rocks.

A number of researchers like Haruna (2017), Woakes *et al.* (1987), Orajaka (1973), Routhier (1976), Olade (1980) etc. have investigated the metallogeny of the Nigerian basement. Also, the presence of coal, limestones, ironstones (Ene *et al.,* 2012; Oladapo and Adeoye-Oladapo, 2011; Ugbor and Okeke, 2010 etc.), and the coexistence of brine fields alongside barite veins and lead-zinc have been documented in the LBT (Uma, 1998). The mineral belts are related to deep seated

structures perhaps outspreading down to the upper mantle (Haruna, 2017). The geologic features function more as channels for hydrothermal fluid movement and mineralization. The intensity, localization, features of hydrothermal mineralization plus the direction and character of groundwater migration are controlled by faults, fractures, fissures etc. (Ekwok *et al*., 2020a; Ekwok *et al.,* 2020b). The enhanced use of geologic concepts and geophysical investigations in a completely integrated programs have been successful in the determination of buried geologic structures and location of new mineral deposits (Woakes *et al.,* 1987). The Nigerian Geological Survey Agency has been in charge of large scale geological mapping and acquisition of airborne geophysical data. These datasets offer a valuable base for further detailed geoscience investigations. Delineation of subtler geologic anomalies are possible because of the availability of high speed and robust computer program (Oha *et al.,* 2016; Elkhateeb and Eldosouky, 2016).

Generally, a lot of geophysical techniques provide a fast approach for exploring near surface magmatic intrusions similar to the ones investigated proximal to brine fields in the Benue Trough (Uma, 1998). Magmatic intrusions which caused hydrothermal variations and structural control are often linked to mineralization (Dill *et al.,* 2010; Airo, 2002). Delineating geologic structures in conjunction with hydrothermally altered rocks are required for mineral prospecting purposes

(Eldosouky *et al.,* 2017). Currently, airborne magnetic and gravity data are considered as key constituents of mineral research programs (Ekwok *et al.,* 2019; USGS 2013, Telford *et al.,* 1990). The mapping of disparities in rock magnetizations and densities are made possible by these data.

The magnetic technique is an effective exploration tool anywhere magnetization is comparatively strong and there are somewhat disparities among the various rock units (Eldosouky and Elkhateeb, 2018). Features such as rock boundaries, surficial regional geologic borders, faults, fractures and dykes can be mapped on enhanced gridded data (Ekwok *et al.,* 2019; Elkhateeb and Eldosouky, 2016). Also, the gravity prospecting is commonly used as a reconnaissance tool in hydrocarbon survey (Kearey *et al.,* 2002, Telford *et al.,* 1990), and constraints in seismic interpretations (Telford *et al.,* 1990). Gravity anomalies can reveal the subsurface form of igneous intrusions (Bott *et al.,* 1958), locate sedimentary basins, and provide important information on mechanisms of basin formation (Kearey *et al.,* 2002). However, it can also be employed in engineering and archaeological investigations (Kearey *et al.,* 2002), hydrogeological search (Ekwok *et al.,* 2020b; Van Overmeeren 1975) and as a follow-up technique applied on a targets well-defined by electromagnetic and magnetic anomalies in joint base-metal explorations (Telford *et al.,* 1990).

This investigation seeks for magnetic and gravity anomalies from variations related to the mineralized regions and/or some certain geologic location of mineralization. In general, it has been documented by several workers that regions of tectonothermal activities and hydrothermal alterations have extensive magnetism and density to the adjoining parts of somewhat free tectonisms (Elkhateeb and Eldosouky, 2016; Gunn and Dentith, 1997; Bott *et al.,* 1958). To reassess mineral potentials of some parts of Southeastern Nigeria, high resolution airborne magnetic and gravity data were employed. In this study, we used image analysis, potential field enhancement methods and 2-D modelling to map hydrothermally modified rock zones, identify probable geological site of mineralization and basin framework in the study area.

1.1 Location of the study area

The investigated area covers some parts of the Cretaceous Lower Benue Trough (LBT) and Precambrian Obudu Plateau (OP). It is part of Enugu, Ebonyi and Cross River States of Southeastern Nigeria. It is positioned between longitude $7^{0}30$'E and $9^{0}00$'E and latitude $6^{0}00$'N and $6^{0}30$'N. The topographic map (Fig. 1) of the region indicates that elevations is in the range of 29.4 -186.5 m with the northwestern and eastern flanks having highest elevations.

1.2 Geologic settings of the study area

Based on geological age, the investigated area occupies two out of the three geological provinces in Nigeria that is, the Precambrian Obudu Plateau and Cretaceous Lower Benue Trough (Fig. 2).

1.2.1 Obudu Plateau

The Nigerian Basement Complex is said to have evolved as a result of a series of tectonothermal happenings of which at least three phases of distortion have been documented (Rahaman and Lancelot, 1984). The basement complex is generally described under three lithologic groups: A migmatite-gneiss complex, the schist belts and older granites sets. The Cretaceous-Recent sedimentary series are well-preserved in structurally controlled basins (Niger Delta, Benue Trough, Calabar Flank, Ikom-Mamfe Rift, Afikpo Syncline, Dahomey, Bida, Sokoto and Chad). The Migmatite-gneiss complexes are thought to be the oldest rocks of the Nigerian Basement Complex (Haruna, 2017). Substantial portion of the complex is understood to be altered older crust of possibly Liberian age, which have been further transformed by later orogenies such as the Eburnean (2000 + 200 Ma) and the Pan African (600+150 Ma) with addition of the schist and granitoids belts (Haruna, 2017). Even though evidence of sedimentation and distortion in Kibaran (1300-1100 Ma) have been described (Haruna and Mamman, 2005), no magmatic event of this age have been documented. The Kibaran was accompanied by ages

ranging from 900-450 Ma signifying the imprint of the Pan-African occurrence which gave rise to gneisses, migmatite, older granite intrusions and related lithologic components (Haruna, 2017). The middle and late Paleozoic age is not represented by any magmatic or depositional event. The Mesozoic is marked by uplift and intrusion of a series of anorogenic, alkaline, shallow sub-volcanic intrusives labelled as the younger Jurrasic granites which fall in a north-south narrow belt in the western part of the eastern province and lengthens north ward towards the Republic of Niger.

The Obudu Plateau which is an annex of the Bamenda Massif, is one of the Nigerian Precambrian basement outcrops in southeast Nigeria (Agbi and Ekwueme, 2018). The lithological disparities in the area involve high grade metamorphic rocks comprising predominantly of schists and gneisses that have been migmatized and intruded by unmetamorphosed dolerites, granites and quartzo-feldspathic veins (Agbi and Ekwueme, 2018). Also, associated with these rocks are insignificant occurrence of amphibolites, metaquartzites and metagabbros. Archaean, Eburnean and Pan-African ages have been gotten from rocks of this area (Ukwang *et al.,* 2012). The relatively close match between the lithology of rocks and ages of the Southeast Nigeria, Northern Cameroon and Central African Fold Belt basement complexes (Ukwang *et al.,* 2012) made researchers to infer that the existences of Nigerian Southeast basement

evolutionary history is related to the Pan-African mobile belt in Central Africa (Agbi and Ekwueme, 2018). The Pan Central African belt in Central Africa is due to a continent-continent collision that involved the northern edge of the Congo Craton as the passive margin and the Adamawa-Yade and western Cameroon domain as the active margin (Agbi and Ekwueme, 2018; Toteu *et al.,* 2004). The OP is dominated by migmatitic gneisses that have been grouped and described as garnet-sillimanite gneiss, garnet-hornblende gneiss, or simply as migmatite gneiss (Agbi and Ekwueme, 2018; Ukwang *et al.,* 2003).

1.2.2 Lower Benue Trough

The tectonic development of southern Nigeria continental basins and indeed, other basins situated in the West and Central African Rift systems, have been traced to the polyphase fragmentation of Gondwana supercontinent in the Late Jurassic to early Cretaceous into the present Africa and South America Plates (Bumby and Guiraud, 2015; Wilson and Guiraud, 1992). This breakup preceded other significant activities like the drifting of the continents and subsequent opening of the South Atlantic. These events were followed by the initiation and development of the mid-Atlantic Ridge. A rise in mantle plume in St Helena Hotspot between 130-100 Ma around the Niger Delta region, which later became the centre of the rift, was a significant tectonic event that generated the pre-

breakup stress of the rocks (Cratchley *et al.,* 1984; Lehner and De Ruiter, 1977; Olade, 1975). Later, additional stresses created by the concurrent outpouring of volcanic fluids from a deep mantle plume linked to the then Tristan da Cunha Hotspot resulted to the final separation of the African and South American Continents between ~100-105Ma. In general, subsidence persisted up to the Santonian that was characterized by repeated phases of widespread regional deformation (Benkhelil *et al.,* 1987). These sequences of rifting, magmatism, thermo-tectonic and extensional events happened at both the continental margin and within the African Continental Plate.

The Benue Trough and all its flanking basins like the Ikom-Mamfe Rift, Anambra Basin, Calabar Flank, Afikpo Syncline, Bida Basin etc. are some of the sedimentary basins that developed from those post breakup tectonic events. Foremost researchers have established that the Benue Trough is a failed arm of the triple junction rift system connected with the parting of Africa from South America in Aptian/Albian period (Cratchley *et al.,* 1984; Burke *et al.,* 1972).

Lower Benue Trough is a fraction of the northeast-southwest trending linear structure called Benue Trough of Nigeria. The region is covered by dense buildup of Cretaceous sedimentary successions deposited under fast changing environments. A series of transgressive-regressive phases in the trough initiated

sedimentation which were influenced by combined effects of eustatic rise in sea level and local diastrophism (Kogbe, 1981). The oldest and basal Asu River Group (ARG) is made up of Abakaliki Shale and Ebonyi Formation. They involve variable thicknesses of shale, siltstone, sandstone, clay and limestone. It may perhaps be that the upper portion of the ARG is of Cenomanian age (Kogbe, 1981), else no sediments of Cenomanian outcrop in the LBT (Agumanu and Enu, 1990). Overlying the ARG is the Turonian Eze-Aku Formation predominated by shales, sandstones and limestone (Agumanu and Enu, 1990). The dark-blue Nkporo/Enugu Formation constitutes part of the pro-deltaic environment which turn out to be even more limited upwards in the Mamu Formation. This is made up of basal coal seams in addition to black shale that is overlain by white fine-coarse-grained Ajali sandstone. It is overlain by interchanging sequences of fine-grained shale and sandstone with some rare coal seams of the Nsukka Formation (Doucet and Popoff, 1985).

3.0 Materials and method

3.1. Data acquisition

The airborne magnetic and gravity data were acquired and assembled by Fugro Airborne Surveys, Canada between 2005 and 2010. These data were collected using Flux-Adjusting Surface Data Assimilation System with flight-line space of 0.1 km, tie line space of 0.5 km and terrain clearance ranging from 0.08-0.1 km

along 826,000 lines. The observed potential field data were of very high resolution when likened to the 1970 aero-geophysical data. These recent potential field data were noticed to be suitable for mineral and petroleum investigations as well as geological mapping.

The regional field in the magnetic and gravity data were subtracted by applying the tenth (10^{th}) generation of International Geomagnetic Reference Field (IGRF) and International Gravity Standardization Net 1971 (IGSN71) Programs respectively, by Fugro Airborne Surveys, Canada. The key benefit of the IGRF and IGSN71 is the consistency they provide in potential field survey practice beginning from when the IGRF and IGSN71 became available and generally accepted (Reeves *et al.,* 1997). Also, they carried out all other required potential field data treatments and reductions. The data used for this study were processed to the form of total magnetic intensity and Bouguer gravity gridded data displayed as imageries in color raster format (Fig. 3).

3.2. Methodology

The potential field data were emptied into the World Geodetic System 84 (WGS 84) and Universal Transverse Mercator coordinate system at zone 32 of Northern hemisphere (UTM 32N) in Oasis Montaj program. The data directories were hosted in MAGMAP, source parameter imaging, Euler deconvolution and GM-

SYS tools which created control files that were employed in the different enhancement and modelling procedures.

Filtering of the potential field data are procedures that consist of enhancing algorithms which carefully attenuate the anomalies from one set of geologic sources relative to anomalies due to other geologic sources (Milligan and Gunn, 1997). Typical potential field data filtering methods consisting of first vertical derivative (Blakely and Simpson, 1986), total horizontal and tilt angle derivatives (Verduzco *et al.,* 2004; Miller and Singh, 1994; Roest *et al.,* 1992; Hood and Teskey, 1989), analytical signal (Roest *et al.,* 1992) and upward continuation (Nabighian, 1984; 1972) were applied in this investigation. To map the spatial distributions, and determine the different anomaly source depths, Euler deconvolution and source parameter imaging (Smith *et al.,* 1998; Thurston and Smith 1997) procedures were done. Likewise, the 2-D joint modelling was used to estimate depth to basement and delineate the basin framework as well as related intrusions and faults.

Computation of the first vertical derivative on potential field data involves the enhancement of near-surface magnetic and gravity sources, and generating an improved resolution of closely-spaced sources (Pal and Majumdar, 2015; Reeves et al., 1997). Higher order vertical derivatives can equally be computed to achieve this effect more, although the noise in the dataset becomes more prominent than

the signal at above the second vertical derivative (Reeves *et al*., 1997). The equation of the wavenumber domain filter to create *nth* derivative is:

$$F(\omega)=\omega^{n} \qquad 1$$

A frequently applied edge detection filter is the total horizontal derivative (THD) (Blakely, 1995; Cordell and Grauch, 1985) and is defined as:

$$THD_{(x,y)}=\left[\left(\frac{\partial A}{\partial x}\right)^{2}+\left(\frac{\partial A}{\partial y}\right)^{2}\right]^{\frac{1}{2}} \qquad 2$$

where A is the magnetic or gravity anomaly, $\frac{\partial T}{\partial x}$ and $\frac{\partial T}{\partial y}$ are the two orthogonal horizontal derivatives of the potential field respectively.

The tilt angle derivative (TDR) is less sensitive to noise than other filtering techniques using higher order derivatives (Akın *et al.,* 2011). It is applied to show the borders of geologic structures generating magnetic and gravity anomalies. TDR is defined as the ratio of the vertical derivative of anomalies to the horizontal derivative. Mathematically it is given as:

$$\theta=\tan^{-1}=\frac{\frac{\partial^{2}A}{\partial z^{2}}}{THD_{(x,y)}} \qquad 3$$

where $THD_{(x,y)}$ is defined in equation 2.

The analytical signal (ASIG) technique (Nabighian, 1984; 1972) creates maximum responses over magnetic and gravity anomalies. This method is typically employed at low magnetic latitude because of the inherent difficulty

related to reduced-to-pole technique. Roest *et al.* (1992) showed that the amplitude of the ASIG can be got from the three orthogonal derivatives of the potential field as:

$$\left|ASIG_{(x,y)}\right| = \sqrt{\left(\frac{\partial A}{\partial x}\right)^2 + \left(\frac{\partial A}{\partial y}\right)^2 + \left(\frac{\partial A}{\partial z}\right)^2} \qquad 4$$

where A is the observed potential field.

Upward continuation method is applied in assessing the regional magnetic and gravity structures coming from deep seated potential field sources. The expression of the wavenumber domain filter to create upward continuation (Telford *et al.,* 1990) is basically:

$$F(\omega) = e^{-h\omega} \qquad 5$$

where is h is the continuation height. This function drops gradually with increasing wave-number, reducing the higher wave numbers more severely, therefore making a map in which the more regional anomalies predominate (Reeves *et al.,* 1997).

The Euler deconvolution technique depend on Euler's homogeneity equation:

$$(x - x_0)\frac{\partial T}{\partial x} + (y - y_0)\frac{\partial T}{\partial y} + (z - z_0)\frac{\partial T}{\partial Z} = N(B - T) \qquad 6$$

where (x_0,y_0,z_0) is the position of a magnetic/gravity source whose total field is observed at (x,y,z), while B is the regional value of the potential field. The

homogeneity degree *N* is taken as a structural index (Reid *et al.,* 1990; Thompson, 1982). Unlike numerous other computer-aided procedures before it, Euler deconvolution doesn't assume any certain geologic model. The procedure can be valued and interpreted even when the geology cannot be appropriately defined by dikes or prisms (Casto, 2001). As well, this process may perhaps be applied directly to the gridded data (Thompson, 1982).

Source parameter imaging (Thurston and Smith, 1997) output are commonly imageries from which depth can be gotten (Smith et al., 1998). This technique evaluates the properties of analytic signal and second derivative responses (Smith et al*.,* 1998). Geologic model can be acquired correctly from the analysis, and just like the Euler deconvolution, depth approximation is not dependent on any assumptions about the geologic model (Smith *et al.,* 1998). Also, the depth solution results are not reliant on the declination and inclination of the magnetic field, so it is inessential to use a reduction-to-pole input grid (Thurston and Smith, 1997). Interpretation procedure involving magnetic and gravity data are made significantly simpler especially when one properly understand the local geology (Thurston and Smith, 1997). The estimations of depth using source parameter imaging is typically from the wavelength of the analytic signal. Nabighian (1972) defined the analytic signal $A_1(x, z)$ as

$$A_1(x,z) = \frac{\partial M(x,z)}{\partial x} - j\frac{\partial M(x,z)}{\partial z} \qquad 7$$

$M(x, z)$ is the magnitude of the anomalous total magnetic/gravity field, j is the imaginary number, and z and x are Cartesian coordinates for the vertical and the horizontal directions perpendicular to the strike, respectively.

Two dimensional forward modelling using the GM-SYS package of Oasis montaj was involved to define depth to basement and delineate the basin framework of the area. The process involves computing the magnetic/gravity responses, creating hypothetical geologic model (Talwani and Heirtzler, 1964; Talwani *et al.*, 1959) and applying the algorithms described by Won and Bevis (1987). The data used for modelling were obtained along carefully drawn two profiles in the East-West direction on the total magnetic intensity and Bouguer gravity datasets (Fig. 3). The profile placements were informed after the various enhancement, Euler deconvolution and source parameter operations were carried out. These procedures served as a guide that ensured profiles were drawn perpendicular to the regional magnetic and gravity anomalies in the investigated area.

4.0 Results

Generally, interpretations involving qualitative and quantitative procedures of potential field data can provide valuable information in mineral explorations, hydrocarbon surveys, archaeological and engineering studies, and can offer constraints in seismic interpretation. Areas predominated by complex geologic structures are ordinarily connected with short wavelength anomalies and

mineralization (Ekwok *et al.,* 2019; Arinze *et al.,* 2019). High frequency filtering involving first vertical derivative (Fig. 4) showed that the OP is defined by compactly packed red-pink colour caused by high density biotite-gneisses and granites (Arinze et al., 2019) characterized by magnetite. An extension of the Ikom-Mamfe Rift (IMR) into the LBT displays high magnetisation and density initiated by Quaternary-Recent tectonism connected to the Cameroun Volcanic Line (Akpan *et al.,* 2014). The anticlinal anomaly that runs in the north-south direction related to the Abakaliki Anticlinorium (AA) in the LBT was properly elucidated by the gravity map (Fig. 4b), and short wavelength locations at the western flank of the area matches very closely (Fig. 4). The total horizontal derivative results (Fig. 5) correlate with Fig. 4, although Fig. 5b successfully delineated source body location, boundary and direction within the investigated area. It displays a collection of symbols in linear pattern signifying the possible nature of contacts between rock units and expressing the different geometrics of the causative bodies. The tilt angle derivative maps (Fig. 6) show lineations (denoted by thin white broken lines) and they are very prominent in the OP and IMR geologic regions. The structures trend majorly in the NE-SW direction (Fig. 6a) and correspond with the direction of the Nigerian Benue Trough. These geologic features are caused by the tectonism that activated the intrusions of unmetamorphosed dolerites, granites and quartzo-feldspathic veins (Agbi and

Ekwueme, 2018; Woakes *et al.,* 1987) and Quaternary-Recent basaltic intrusions (Ekwok *et al.,* 2019; Akpan *et al.,* 2014) into the Precambrian basement and Cretaceous sediments of the OP and IMR respectively. In addition, Fig. 6b validates the findings of Fig. 5b.

To detect the limits of magnetic and gravity source bodies, analytical signal procedure was carried out on the magnetic and gravity data (Fig. 7). The process creates maximum directly over discrete bodies as well as their edges (Elkhateeb and Eldosouky, 2016). From analytic signal results, magnetic and gravity low (blue) and high (red-pink) intensities can easily be noticed. Apart from the OP and IMR (Fig. 7a) with high intensities, they exist short wavelength structures (described by red-pink) unevenly distributed in the LBT representing dyke-like basic and intermediate intrusions. Also, some pockets of low magnetic and density signatures characterized by various blue colours specify the locations of long wavelength anomalies. To assess these tectonic structures clearly, the magnetic and gravity datasets were upward continued to 5000 m (Fig. 8) to remove the magnetic and gravity effects emanating from near-surface geologic sources. This filtering procedure elucidates the main crustal blocks and intrusions that exist in the region. Fig. 8a shows deeply buried N-S trending intrusive body (described by red-pink colour) that coincide with location of the Abakaliki Anticlinorium. This structure extended to the western flank (Fig. 8b) of the study

area. Similarly, the eastern end of the study area that matches with the OP region is dominated by deeply buried high magnetisation and density structure that trends in the NE-SW direction although, Fig. 8a feature stretches up to the Ndibinaofia in the NW-SE direction. The extensive major tectonics observed in the area are related to the previously reported Santonian and Quaternary-Recent tectonic activities of the area (Agbi and Ekwueme, 2018; Oha *et al.,* 2016; Woakes *et al.,* 1987; Benkhelil, 1987; Burke and Dewey, 1974). Also, Fig. 8b showed distinctly the NE-SW weak zone (defined by blue and lemon green colours) that trends in the same direction with the Nigerian Benue Trough. The structure represents the border between the Precambrian basement and the Cretaceous sediments.

The Euler deconvolution and source parameter were applied on the potential field data to determine the locations and depths of anomalies of geologic origin (Figs. 9 and 10). The gridded imageries show wide-ranging colours indicating different magnetic susceptibility and density contrast in the investigated area. The map successfully showed the distribution of deep and shallow magnetic and gravity sources in the investigated area. According to Thurston *et al.* (2002), the negative sign in the colour legend bar signifies depth measurement from the Earth's surface downward. The various results revealed depths in the range of ~13.0 m to ~2570.2 m. The main blue colour zone (with depths more than ~2000 m)

located at the neighbourhood of Bansara (Figs. 9 and 10) and some pockets of blue colour scattered all over in the investigated area indicates low frequency structures. The Precambrian OP and Cretaceous IMR as well as regions that have experienced some minor tectonic events (Agbi and Ekwueme, 2018; Oha *et al.,* 2016; Akpan *et al.,* 2014; Woakes *et al.,* 1987) are thinly covered by sediments (~13.0 – ~942.9 m), whereas intermediate depths in the range of ~942.9 and ~1782.9 m were witnessed over the remaining areas.

The potential field curves gotten from the 2-D models (Figs. 11 and 12) are defined by breaks on the signatures. These breaks show key weak zones within the basement rocks that created spaces for magmatic intrusions. The positions of these lineaments match closely with each other signifying the extended nature of the weak zones. The lineament system are regarded as syn-rift structures initiated during the rifting episode that created the Cretaceous Benue Trough and other inland sub-basins (Ekwok *et al.,* 2020a; Ekwok *et al.,* 2019). Also, towards the eastern flank of these models, the breaks indicate the border line between the OP and LBT. The major post-depositional intrusions that defined the Abakaliki Anticlinorium and Ikom-Mamfe Rift were captured around Okpoto-Agu and Igboji, and close to Mbok and Agbaragba (Figs. 11 and 12) areas respectively. These geologic structures related to the Santonian Abakaliki Anticlinorium (Ekwok *et al.,* 2020a) and Quaternary-Recent Cameroun Volcanic Line (Akpan

et al., 2014) caused extensive uplifts, faulting, fracturing and baking of sedimentary series (Ekwok *et al.,* 2020b; Arinze *et al.*, 2019; Oha *et al.,* 2016) in these locations and adjoining areas. Fig. 11 captured a dyke-like structure in the OP basement suspected to be dolerite, granite or quartzo-feldspathic intrusion (Agbi and Ekwueme, 2018). From the depth results obtained from Figs. 11 and 12, the sediment thicknesses are generally less than 3000 m. Extrusive basaltic rock previously reported by Ekwok *et al.* (2019) in the IMR was observed within Agbaragba in the IMR whereas the OP basement outcropped near Kakube. The OP basement is reported to have witnessed tectonic disturbances creating geologic structures intruded by dolerites, granites and quartzo-feldspathic (Agbi and Ekwueme 2018; Haruna, 2017; Woakes *et al.,* 1987; Orajaka, 1973; Routhier, 1976 and Olade, 1980).

5.0 Discussion

The investigation area characterized by tectonothermal events is dominated by varied forms of long and short wavelength anomalies of geologic origin. The metallogeny of the basement rocks (Haruna, 2017; Woakes *et al.,* 1987; Orajaka, 1973; Routhier, 1976; Olade, 1980) and the existence of coal, ironstones, limestones and the simultaneity of brine fields near lead-zinc and barite veins in the LBT (Ene *et al.,* 2012; Oladapo and Adeoye-Oladapo, 2011; Ugbor and Okeke, 2010; Uma, 1998) have been studied and well documented. Regions of

dense concentrations of high frequency anomalies caused by tectonisms were properly revealed by the enhanced magnetic results (Figs. 4a, 5a and 6a). The short wavelength anomalies are compactly packed in the IMR and OP geologic regions. These findings which agreed with the results obtained by Arinze *et al.* (2019) and Oha *et al.* (2016). These regions described as hydrothermally altered (Ekwok *et al.,* 2020a; Oha *et al.,* 2016) are characterized by faults, fractures, fissures, dykes, sills and baked Albian shales (Ekwok *et al.,* 2019). Likewise, similar enhancement on the Bouguer gravity data (Figs. 4b, 5b and 6b) mapped clearly the N-S trending Santonian Abakaliki Anticlinorium (Oha *et al.,* 2016; Benkhelil, 1987), Quaternary-Recent basaltic intrusions (Akpan *et al.,* 2014), and Precambrian OP rich in magnetite and intruded by dolerites, granites and quartzo-feldspathic (Agbi and Ekwueme, 2018; Haruna, 2017; Woakes *et al.,* 1987). The origin of these high frequency anomalies (Figs. 4a, 5a and 6a) were elucidated by Figs. 7 and 8. These anomalies (Figs. 4, 5 and 6) are linked to the main tectonic structures of the area (Figs. 7 and 8) possibly extending to the upper mantle (Haruna, 2017). These geologic structures function as pathways for hydrothermal fluids (super enriched metalliferous brines) migration (Mineral resources of the western US, 2017; USGS, 2013; Dill *et al*., 2010; Airo, 2002; GSC, 1994 and GSC, 1992) and deposition.

Sediment thicknesses results which were generally observed to be less than 3000 m (Figs. 9, 10, 11 and 12) correlate strongly with each other. In the LBT, researchers have estimated depth in the range of ~2.5-8.0 km (Ekwok *et al.,* 2020a). The thin sedimentations observed in the area is due to the proliferation of post-depositional intrusions (Figs. 9 and 10) in this part of the LBT (Ekwok *et al.,* 2019; Arinze *et al.,* 2019; Akpan *et al.,* 2014) and massive outcrops of the basement in the OP (Agbi and Ekwueme, 2018; Ukwang *et al.,* 2012). The 2-D models (Figs. 11 and 12) mapped the depth, basin topography and showed the locations of the intrusions associated with the AA, IMR and OP. These magmatic intrusions which have been revealed by Figs. 7 and 8, have considerably boosted the geothermal gradients and initiated doming, baking and deformation of overlying Cretaceous sediments (Ekwok *et al.,* 2019; Akpan *et al.,* 2014). They are several reports that magmatism is related to mineralization (Ekwok *et al.,* 2020a; Ekwok *et al*., 2019; Arinze *et al.,* 2019; Mineral resources of the western US, 2017; USGS, 2013; Haruna, 2017; Dill *et al*., 2010; Airo, 2002; GSC, 1994; GSC, 1992 etc.). Igneous intrusions are believed to be responsible for large deposits of base metals and brine fields in the LBT. Also, the OP seems to be a feasible site for metallogenic mineral exploration.

6.0 Conclusion

Potential field data enhancement and modelling procedures adopted elucidated short and long wavelength structures initiated by tectonic events in the investigation area. The main tectonics of the area were imaged, and they are believed to be the main caused of short wavelength structures prominently observed in the IMR and OP geologic regions. Relatively thin (~13.0 to <3000 m) sedimentation covers the basement and intrusive rocks. This is caused by the extensive outcropped Precambrian basement in some locations in the OP and the proliferation of magmatic intrusions in the LBT. The 2-D GM-SYS joint models revealed the underlying basement topography, the site of intrusions, anticlinal structures and related normal faults. These intrusions and associated geologic structures are commonly associated with base metal, brine and metallogenic mineralizations.

References

Agbi, I. & Ekwueme, B. N., (2018). Preliminary review of the geology of the hornblende biotite gneisses of Obudu Plateau Southeastern Nigeria. Global Journal of Geological Sciences, 17, 75-83.

Airo, M. L., (2002). Aeromagnetic and aeroradiometric response to hydrothermal alteration. *Surveys in Geophysics, 23*, 273–302.

Akın, U., Şerifoğlu, B.I. & Duru, M., (2011). Using the tilt angle in gravity and magnetic methods. *Bulletin of the Mineral Research and Exploration*, 143, 1-12.

Akpan, A. E., Ebong D. E., Ekwok S.E. & Joseph, S., (2014). Geophysical and Geological Studies of the Spread and Industrial Quality of Okurike Barite Deposit. *American Journal of Environmental Sciences*, 10 (6), 566-574

Benkhelil, J., (1987). The Origin and Evolution of the Cretaceous Benue Trough (Nigeria), Journal of African Earth Science, 8(2-4), 251-282.

Blakely, R. J., (1995). *Potential Theory in Gravity and Magnetic Applications*. Cambridge: Cambridge University Press.

Blakely, R.J. & Simpson, R.W., (1986) Approximating edges of source bodies from magnetic or gravity anomalies, *Geophysics*, 51, 1494-1498.

Bott, M. H. P., Day, A. A. & Masson-Smith, D., (1958). The geological interpretation of gravity and magnetic surveys in Devon and Cornwall. *Phil.Trans. R. Soc.*, 215A, 161–91.

Bumby, A. J., & Guiraud, R., (2005). The Geodynamic Setting of the Phanerozoic Basins of Africa. Journal of African Earth Sciences, 43, 1-12.

Burke, K. C. A. & Dewey, J. F., (1974). Two plates in Africa during the Cretaceous? *Nature*, 249: 313-316.

Burke, K. C., Dessauvagie, R. F. J., & Whiteman, A. W., (1972). Geological history of the Benue valley and adjacent areas. In: Dessauvajie, T. F. J., and Whiteman, A. J. (eds). African Geology, University of Ibadan Press. pp. 187-206.

Casto, D. W., (2001). Calculating depths to shallow magnetic sources using aeromagnetic data from the Tucson basin. *Open-File Report*, 01-505.

Cordell, L., Grauch, V. J. S., (1985). Mapping basement magnetization zones from aeromagnetic data in the San Juan basin, New Mexico. In The Utility of Regional Gravity and Magnetic Anomaly Maps; Hinzc, W.J., Ed.; Society of Exploration Geophysicists: Tulsa, OK, USA, 181–197.

Cratchley, C. R., Louis P., & Ajakaiye, D. E., (1984). Geophysical and Geochemical Evidence for the Benue Chad Basin Cretaceous Rift Valley

System and its Tectonic Implications. Journal of African Earth Science, 2(2), 141-150.

Dentith, M. C., Cowan, D. R. & Tompkins, L. A., (2000). Enhancement of subtle features in aeromagnetic data. *Exploration Geophysics,* 31 (1/2), 104-108.

Dill, H. G., Botz, R., Berner, Z. & Hamad, A. B. A., (2010). The origin of pre- and synrift, hypogene Fe-P mineralization during the Cenozoic along the Dead Sea Transform Fault, Northwest Jordan. *Economic Geologist*, *105*, 1301–1319.

Doucet, J. F., & Popoff, M., (1985). Rapport de mission 1984-1985. Bassins d'Anambra (partie nord) et d'Afikpo. Trav. Lab. Sei. Terre, *Marseille St-Jerome*, 86, 46.

Ekwok, S. E., Akpan, A. E. & Ebong, D. E., (2019). Enhancement and modelling of aeromagnetic data of some inland basins, southeastern Nigeria. *Journal of African Earth Sciences*, 155, 43-53.

Ekwok, S. E., Akpan, A. E. & Kudamnya, E. A., (2020a). Exploratory mapping of structures controlling mineralization in Southeast Nigeria using high resolution airborne magnetic data. J*ournal of African Earth Sciences*, 162, 103700.

Ekwok, S. E., Akpan, A. E. Kudamnya, E. A. & Ebong D. E., (2020b). Assessment of groundwater potential using geophysical data: a case study in parts of Cross River State, south-eastern Nigeria. Applied Water Science, 10:144. Doi.org/10.1007/s13201-020-01224-0.

Eldosouky, A. M. & Elkhateeb, S. O., (2018). Texture analysis of aeromagnetic data for enhancing geologic features using co-occurrence matrices in Elallaqi area, South Eastern Desert of Egypt. *NRIAG Journal of Astronomy and Geophysics* 7 (2018) 155-161.

Eldosouky, A. M., Abdelkareem, M. & Elkhateeb, S. O., (2017). Integration of remote sensing and aeromagnetic data for mapping structural features and hydrothermal alteration zones in Wadi Allaqi area, South Eastern Desert of Egypt. *Journal of African Earth Sciences,* doi: 10.1016.

Elkhateeb, S. O. & Eldosouky. A. M., (2016). Detection of porphyry intrusions using analytic signal (AS), Euler Deconvolution, and Centre for Exploration Targeting (CET) Technique Porphyry Analysis at Wadi Allaqi Area, South Eastern Desert, Egypt. *International Journal of Engineering Research*, 7(6), 471-477.

Ene, E. G., Okogbue, C. O. & Dim C. I. P., (2012). Structural styles and economic potentials of some barite deposits in the Southern Benue Trough, Nigeria. *Romanian Journal of Earth Sciences,* 86 (1), 27-40.

Enu, E. I., Adegoke, O. S, Robert, C., Ako, B. D., Ajayi, T. R., Adediran, S. A. & Oriyomi, A., (1981). Clay mineral distribution in the Nigerian tar sand sequence: Developments in sedimentology (Eds van Olphen, H & Veniale, F.) 35. *Elsevier, Amsterdam*, 321-33.

Geological Survey of Canada (GSC), (1992). Airborne geophysical survey, Mount Milligan area, British Columbia (NTS 93 O/4W, N/1, N/2E); GSC Open File 2535.

Geological Survey of Canada (GSC), (1994). Airborne geophysical survey, Selwyn River, Yukon Territory, (NTS 115I/12W, J/9, J/10, and parts of J/11, 12, 13); GSC Open File 2816.

Gunn, P. J. & Dentith, M. C., (1997). Magnetic responses associated with mineral deposits. *AGSO Journal of Australian Geology and Geophysics* 17, 145-158.

Haruna, I. V. & Mamman, Y. D., (2005). A Brief Review of Some Metallogenetic Features of Uranium Mineralisation in the Upper Benue Trough, N.E. Nigeria. *Technology and Development Journal,* 9*,* 1–8

Haruna, I. V., (2017). Review of the Basement Geology and Mineral Belts of Nigeria. *Journal of Applied Geology and Geophysics,* 5(1), 37-45.

Hood, P. J. & Teskey, D. J., (1989). Aeromagnetic gradiometer program of the geological survey of Canada. *Geophysics*, 54(8), 1012-1022.

Kearey, P., Brooks, M. & Hill, I., (2002). *An introduction to geophysical exploration* (3rd edition). New York: Blackwell Science Ltd Editorial Offices

Kogbe, C. A., (1981). Major transgressive episodes in the Benue Valley of Nigeria. *Earth Evolution Science* 6 (2), 144-148.

Kogbe, C. A., (1981). Major transgressive episodes in the Benue Valley of Nigeria. *Earth Evolution Science* 6 (2), 144-148.

Lehner, P. & De Ruiter, P. A. C., (1977). Structural history of Atlantic Margin of Africa: American Association of Petroleum Geologists Bulletin, 61, 961-981.

Miller, H. G. & Singh, V., (1994). Potential field tilt -A new concept for location of potential field sources: Journal of Applied Geophysics, 32, 213–217.

Milligan, P. & Gunn, P., (1997). Enhancement and presentation of airborne geophysical data. *AGSO J. Aust. Geol. Geophys*, 17 (2), 63–75.

Mineral resources of the western US (2017). The teacher-friendly guide to the Earth scientist of the Western US. http:/ /geology. Teacher friendly guide. Org /index. php/ mineral-w.

Nabighian, M. N., (1972). The analytical signal of two dimensional magnetic bodies with polygon cross-section: Its properties and use for automated anomaly interpretation: *Geophysics, 37*, 507-517.

Nabighian, M. N., (1984). Towards the three-dimensional automatic interpretation of potential field data via generalized Hilbert transforms. Fundamental relations: *Geophysics, 53*, 957-966.

Oha, I. A., Onuoha, K. M., Nwegbu, A. N. & Abba, A. U., (2016). Interpretation of high resolution aeromagnetic data over southern Benue Trough, southeastern Nigeria. *J. Earth Syst. Sci.,* 125, (2) 369–385.

Oladapo, M. I. & Adeoye-Oladapo, O. O., (2011). Geophysical investigation of barite deposit in Tunga, Northeastern Nigeria. *Int. J. Phys. Sci.,* 6: 4760-4774.

Olade, M. A., (1975). Evolution of Nigeria's Benue trough (Aulacogen): a tectonic model. Geological Magazine, 112, 575 - 583.

Olade, M. A., (1980). Precambrian metallogeny in West Africa. Geol., *Rundsch.* 69, 411-428.

Orajaka, S. O., (1973). Possible metallogenic provinces in Nigeria. *Econ. Geol*., 68, 278-280.

Pal, S. K. & Majumdar, T. J., (2015). Geological appraisal over the Singhbhum-Orissa Craton, India using GOCE, EIGEN6-C2 and in situ gravity data. *International Journal of Applied Earth Observation and Geoinformation, 11*, 155-166.

Rahaman M. A. & Lancelot J. R., (1984). Continental crust evolution in SW Nigeria: constraints from U/Pb dating of pre-Pan-African gneisses. In Rapport d'activite 1980–1984 Documents et Travaux du Centre Geologique et Geophysique de Montpellier, 41-50.

Reeves, C., Reford, S., & Millingan, P., (1997). Airborne geophysics:old methods, new images. In: Gubins, A. (Ed.), Proceedings of the Fourth Decennial *International Conference on Mineral Exploration*, 13–30 (Australia).

Reid, A. B., Allsop J. M., Granser, H., Millett, A. J. & Somerton, I. W., (1990). Magnetic interpretation in three dimensions using Euler deconvolution. *Geophysics*, 55, 80–91.

Reyment, R. A., (1965). *Aspects of the Geology of Nigeria*. Ibadan University Press, Ibadan, 445.

Roest, W. R., Verhoef, J., Pilkington, M., (1992). Magnetic interpretation using the 3-D analytic signal. *Geophysics*, 57(1), 116-125.

Routhier, P., (1976). The distribution in space and time of mineral deposits (metallic and metallogenic provinces). In: Colloque C. I., Ressources minerales, du 26 ° C.G.I., 79-80.

Smith, R. S., Thurston, J. B., Dai, T. & MacLeod, I. N., (1998). iSPI™ the improved source parameter imaging method[1]. *Geophysics Prospecting*, 46, 141-151.

Talwani, M. & Hiertzler, J. R., (1964). Computation of magnetic anomalies caused by two dimensional bodes of arbitrary shape. *Geol. Sci.,* 9, 464-480.

Talwani, M., Worzel, J. L. & Landisman, M., (1959). Rapid gravity computations for 2 dimensional bodies with application to the Mendocino submarine fracture zone. *J. Geophys. Res.,* 64, 49-59.

Telford, W. M, Geldart, L. P. & Sheriff, R. E., (1990). *Applied geophysics* (2nd edition). Cambridge: Cambridge University Press.

Thompson, D. T., (1982). EULDPH: A new technique for making computer-assisted depth estimates from magnetic data. *Geophysics*, 47, pp. 31-37.

Thurston**,** J. B. & Smith, R. S., (1997). Automatic conversion of magnetic data to depth, dip, and susceptibility contrast using SPI™ method. *Geophysics,* 62, 807-813.

Thurston, J. B., Smith, R. S. & Guillon, J. C., (2000). A multi-model method for depth estimation from magnetic data: Geophysics*, 67,* 555–561.

Toteu, S. F., Penaye, J. & Djomani, Y. P., (2004). Geodynamic evolution of the Pan-African belt in Central Africa with special reference to Cameroon. *Canadian Jour. Earth Sci*. 41: 73–85.

Ugbor, D. O. & Okeke, F. N., (2010). Geophysical investigation in the Lower Benue Trough of Nigeria using gravity method. *International Journal of the Physical Sciences*, 5(11), 1757-1769.

Ukwang, E. E, Ekwueme, B. N. & Kröner, A., (2012). Single zircon evaporation ages: Evidence for the Mesoproterozoic crust in S.E. Nigerian basement complex. *Chin. J. Geochem*. 31, 48-54.

Ukwang, E. E., Ekwueme, B. N. & Horsley, R. J., (2003). Petrology of the granulite facies rocks in Ukwortung area of Obudu plateau, southeastern Nigeria. *Global. J. Geol. Sci.,* 1(2), 159-167.

Uma, K. O., (1998). The brine fields of the Benue Trough, Nigeria: a comparative study of geomorphic, tectonic and hydrochemical properties. *Journal of African Earth Sciences,* 26 (2), 261-275.

United States Geological Survey (USGS), (2013). Setting and origin of iron oxide-copper-cobalt-gold-rare earth element deposits of southeast Missouri: http://minerals.usgs.gov/east/semissouri/index.html.

Van Overmeeren, R. A., (1975). A combination of gravity and seismic refraction measurements, applied to groundwater explorations near Taltal, Province of Antofagasta, Chile. *Geophys. Prosp.*, 23, 248–58.

Verduzco, B., Fairhead, J. D. Green, C. M. & MacKenzie, C., (2004). New insights into magnetic derivatives for structural mapping. *The Leading Edge*, 23, 116–119.

Wilson, M. & Guiraud, R., (1992). Magmatism and rifting in Western and Central Africa, from Late Jurassic to Recent times. In: P.A. Ziegler (Editor), Geodynamics of Rifting, Volume II. Case History Studies on Rifts: North and South America and Africa. Tectonophysics, 213, 203-225.

Woakes, M., Rahaman, M. A. & Ajibade, A. C., (1987). Some metallogenetic features of the Nigerian Basement. Journal of African Earth Sciences, 6, 5, 655-664.

Won, I. J. & Bevis, M., (1987). Computing the gravitational and magnetic anomalies due to a polygon: algorithms and Fortran subroutines. *Geophysics,* 52, 232-238.

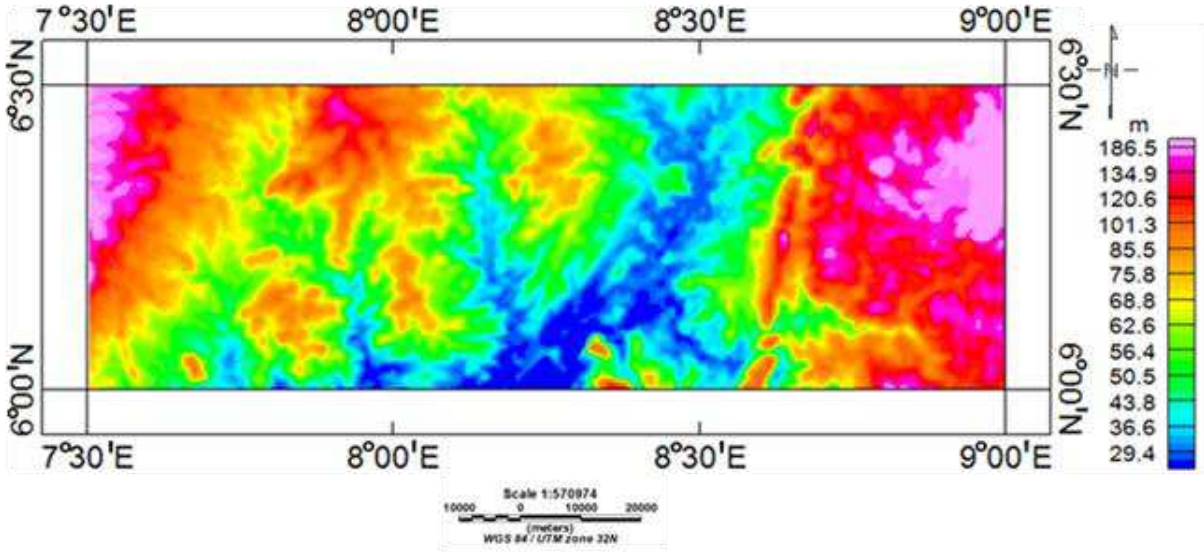

Fig. 1: Digital elevation map of the study area.

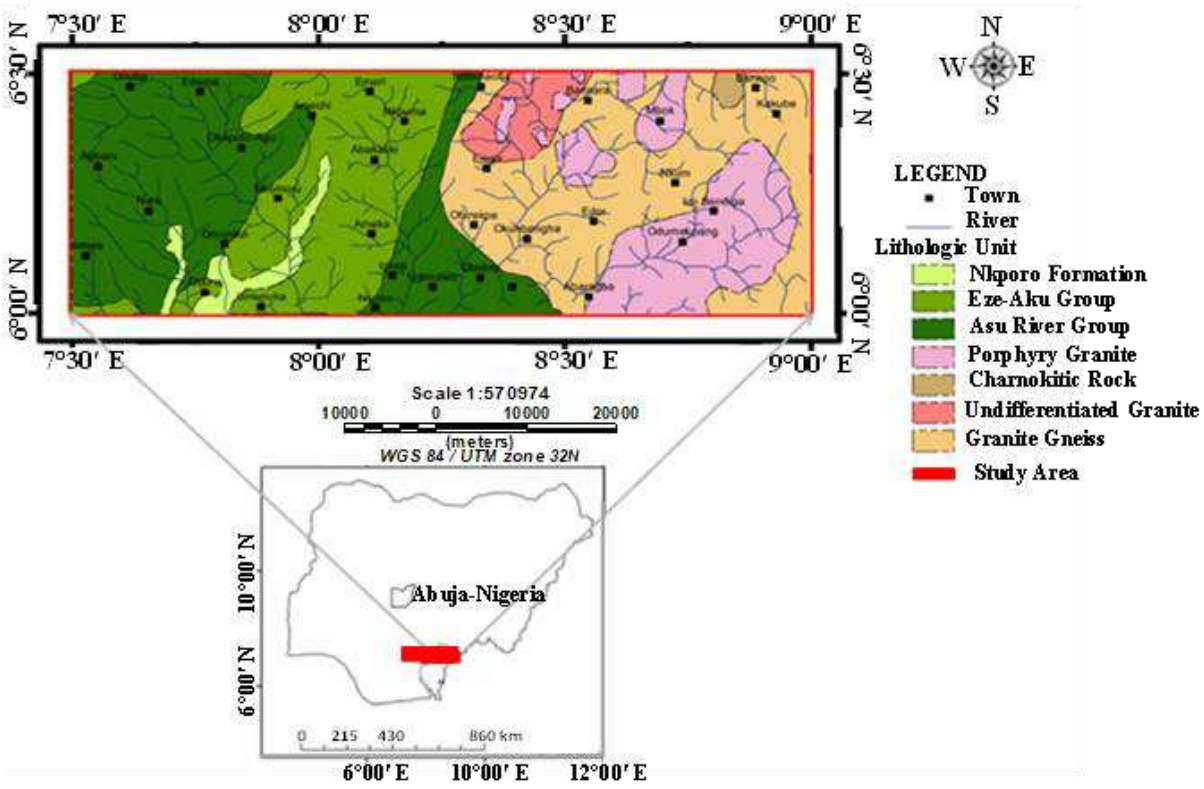

Fig. 2: Geologic map of the study area.

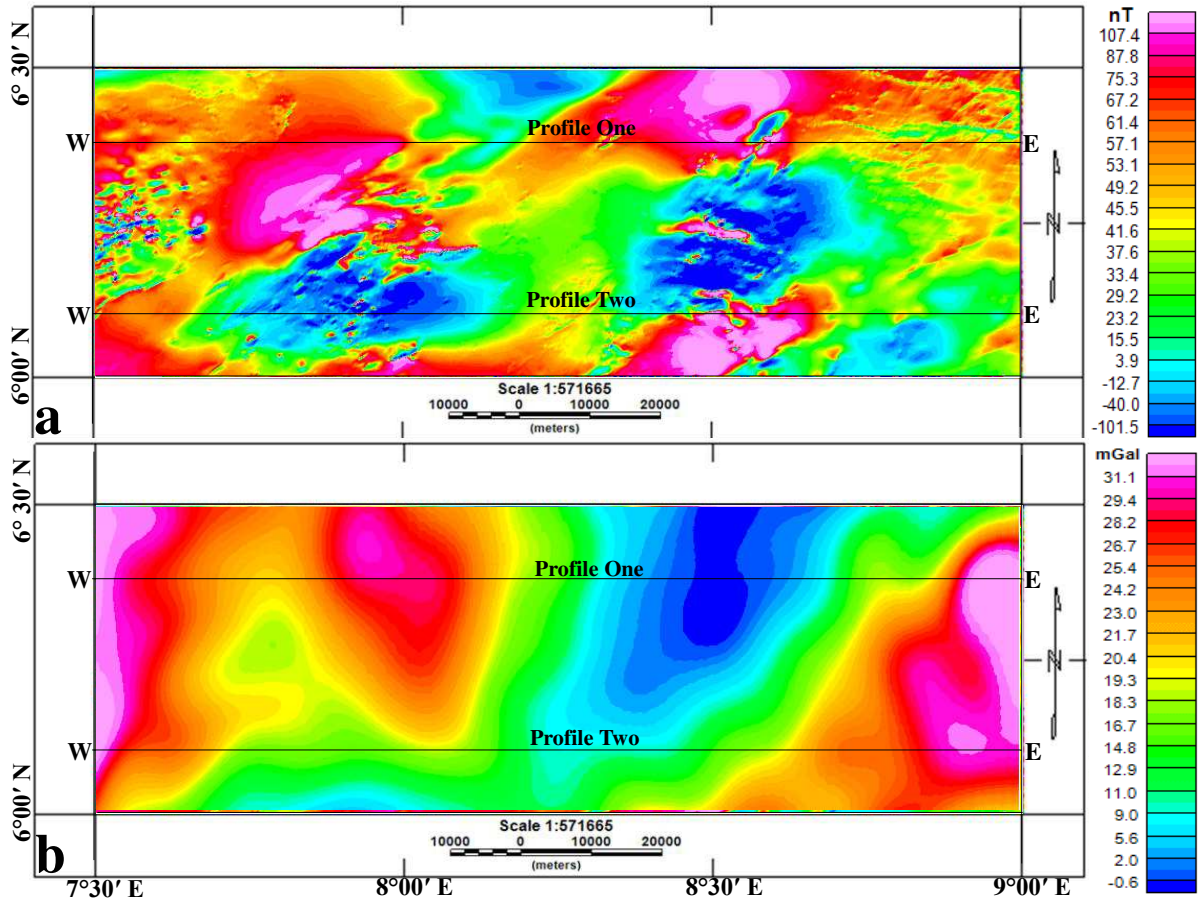

Fig. 3: (a) Total magnetic intensity and (b) Bouguer gravity gridded maps.

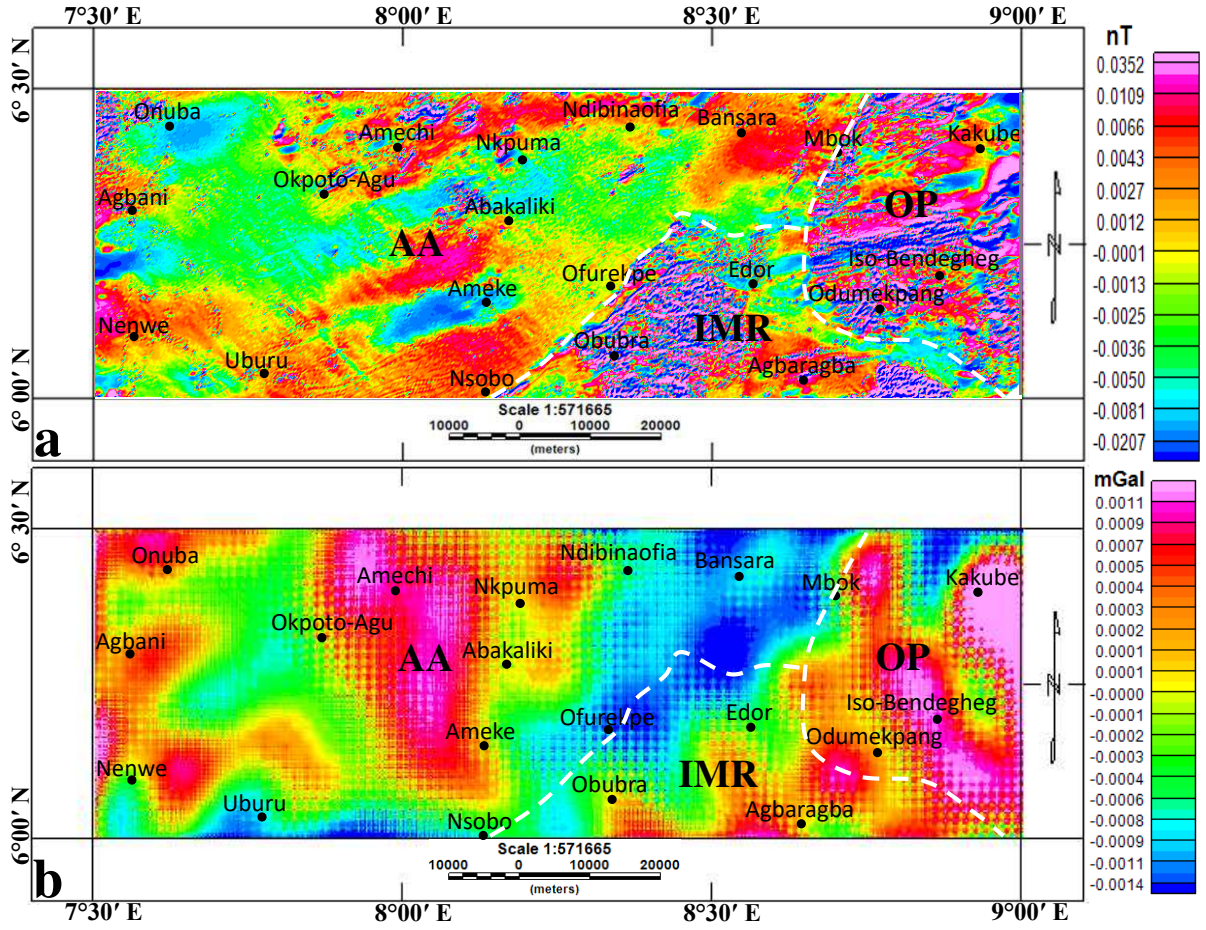

Fig. 4: First vertical derivative maps of (a) total magnetic intensity and (b) Bouguer gravity data.

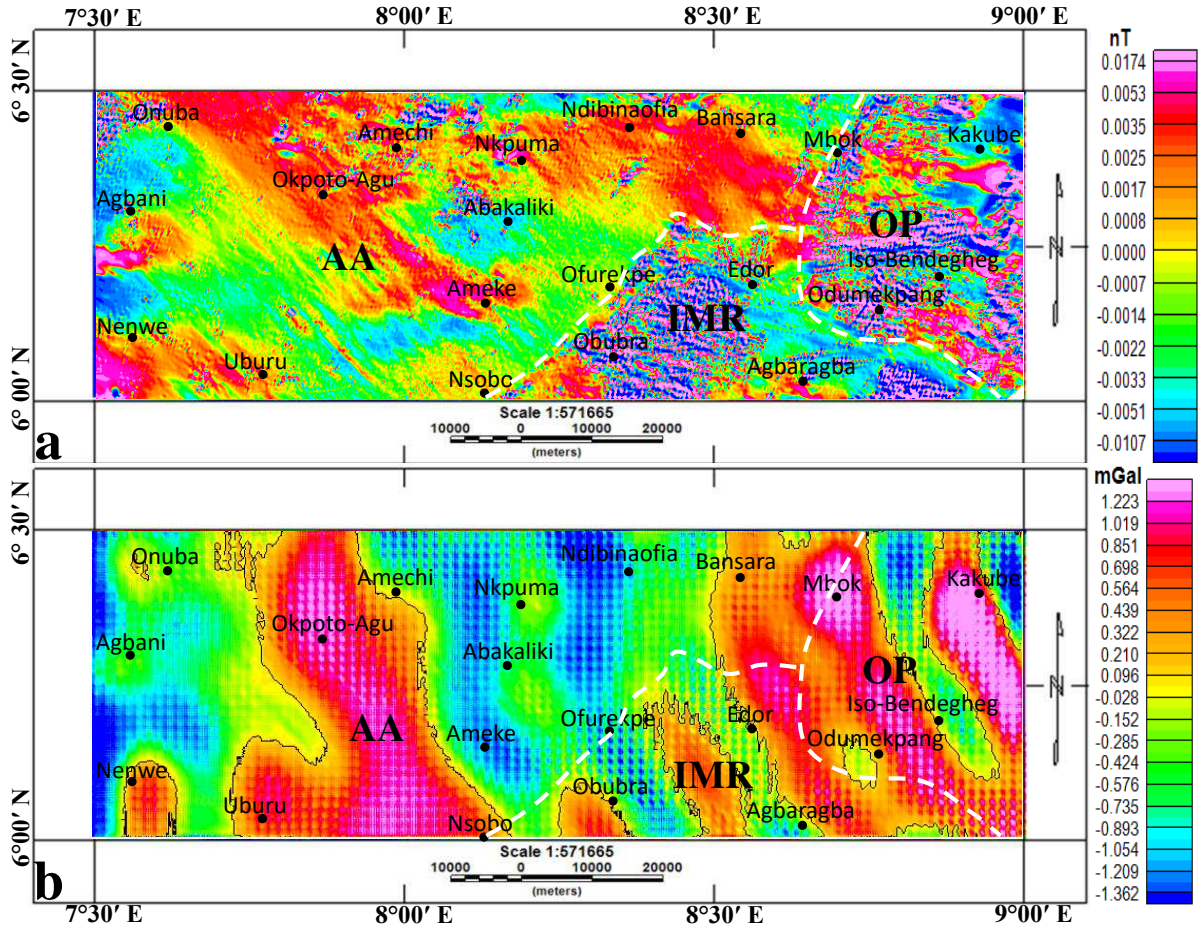

Fig. 5. Total horizontal derivative maps of (a) total magnetic intensity and (b) Bouguer gravity data.

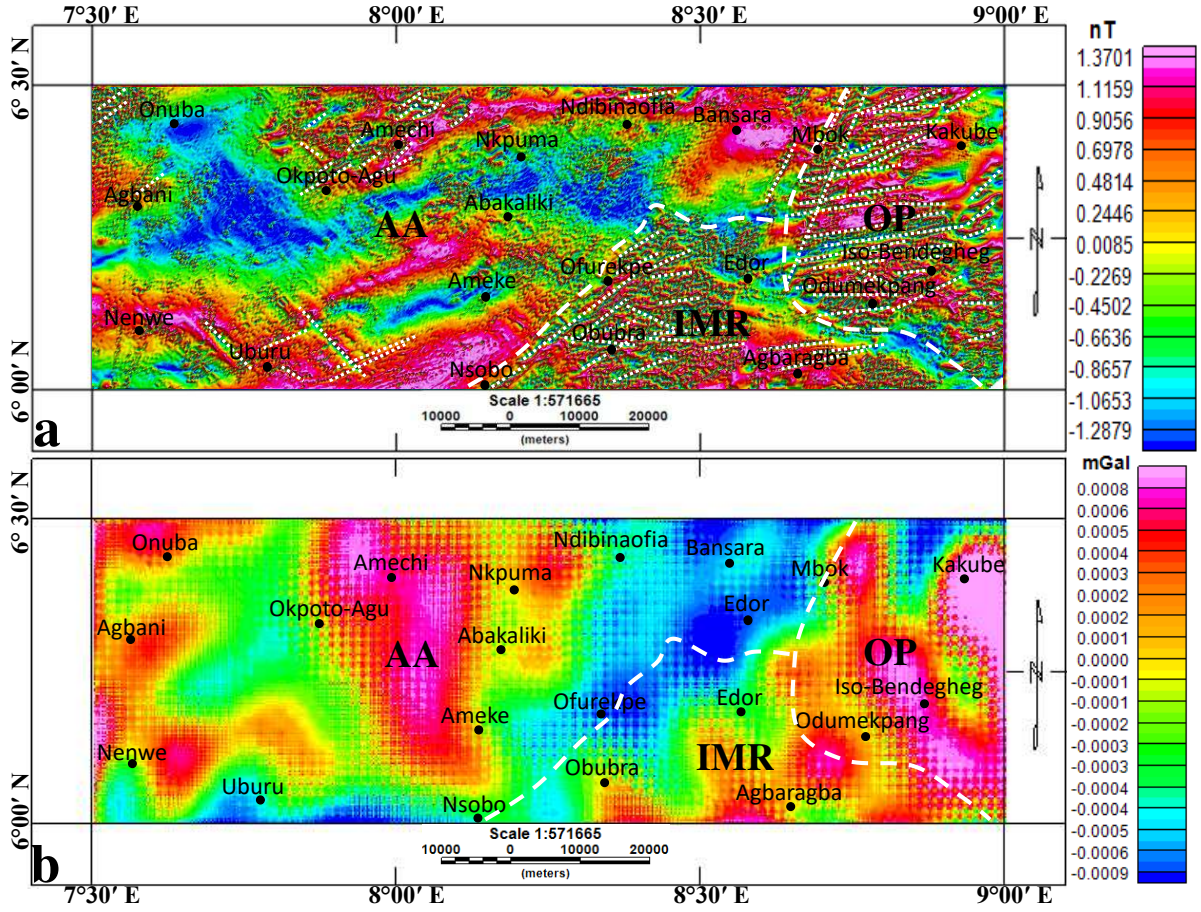

Fig. 6: Tilt angle derivative maps of (a) total magnetic intensity and (b) Bouguer gravity data.

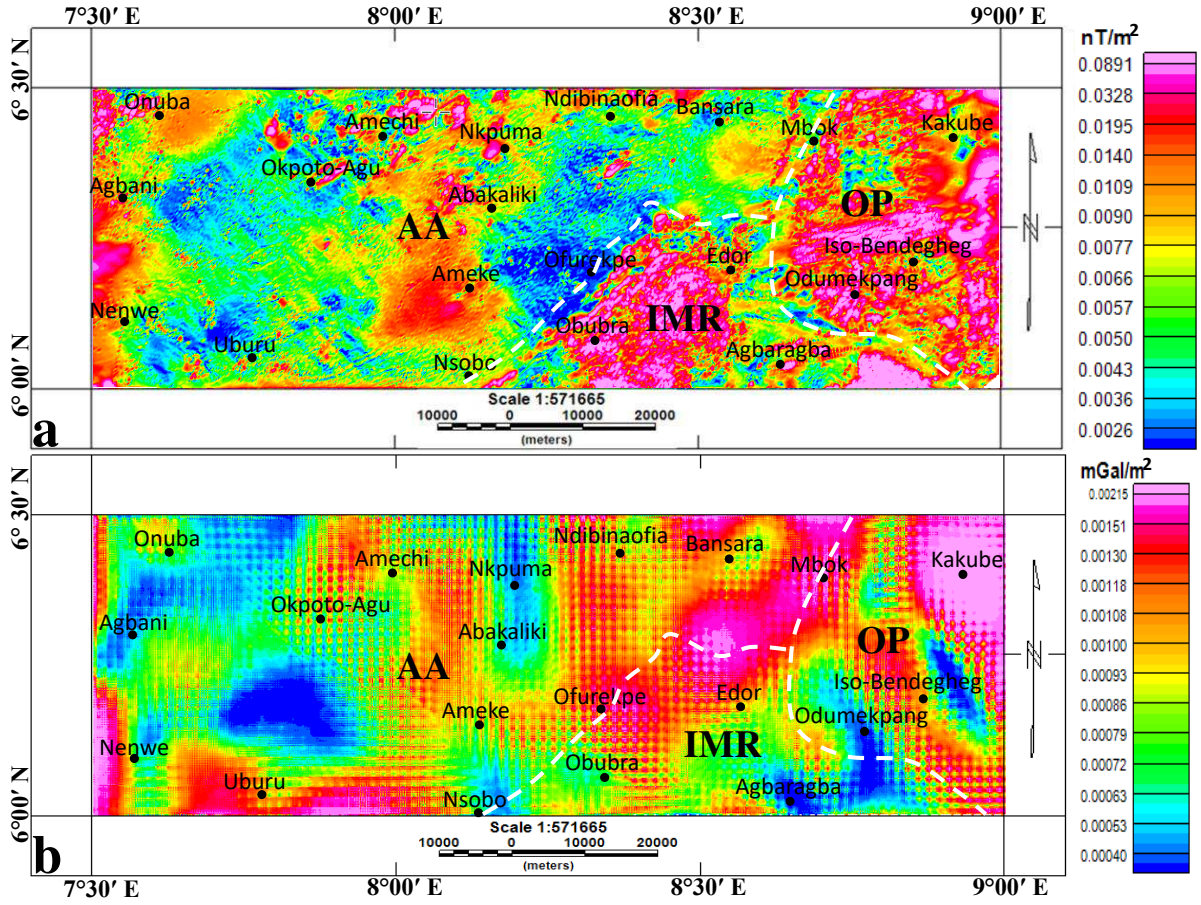

Fig. 7: Analytic signal maps of (a) total magnetic intensity and (b) Bouguer gravity data.

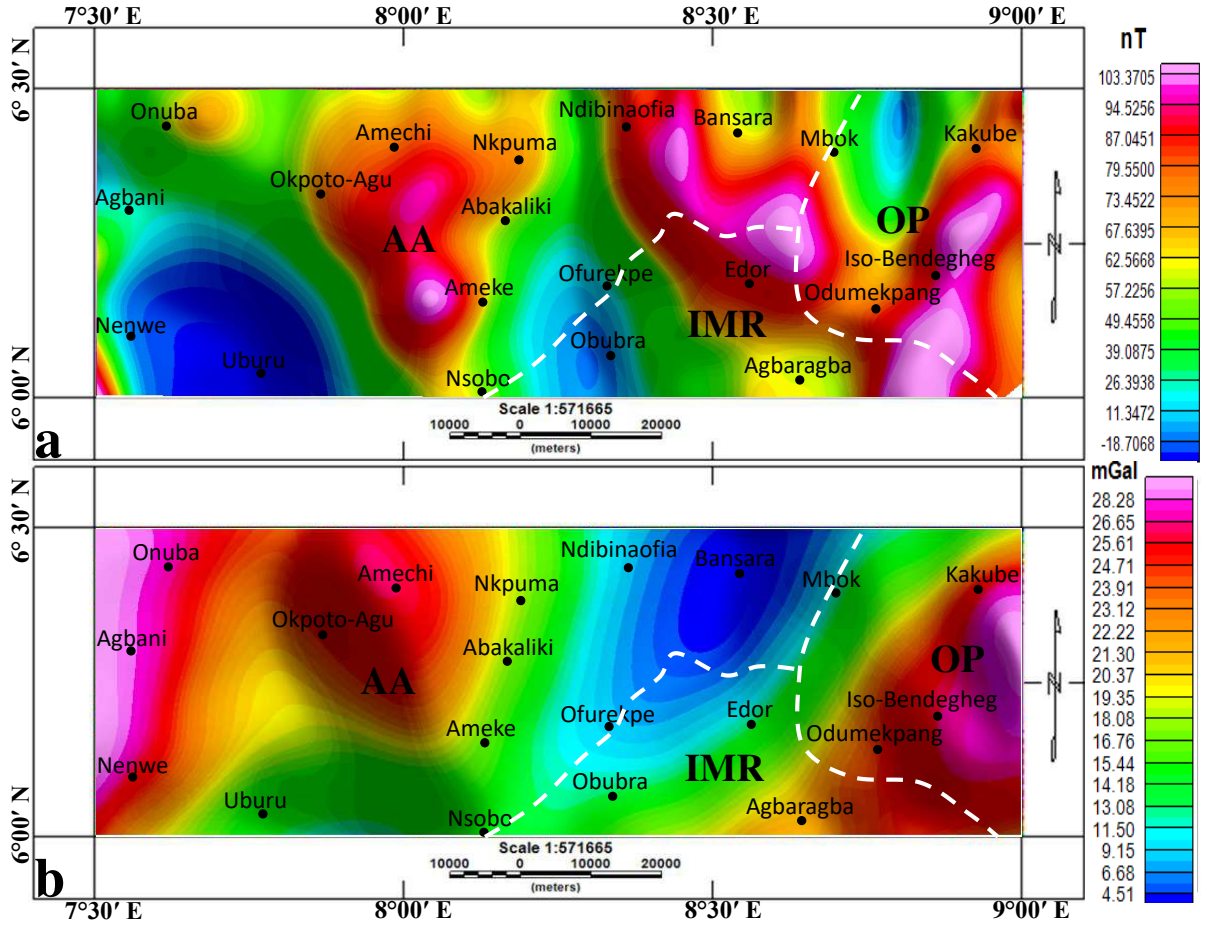

Fig. 8: Upward continued to 5000 m maps of (a) total magnetic intensity and (b) Bouguer gravity data.

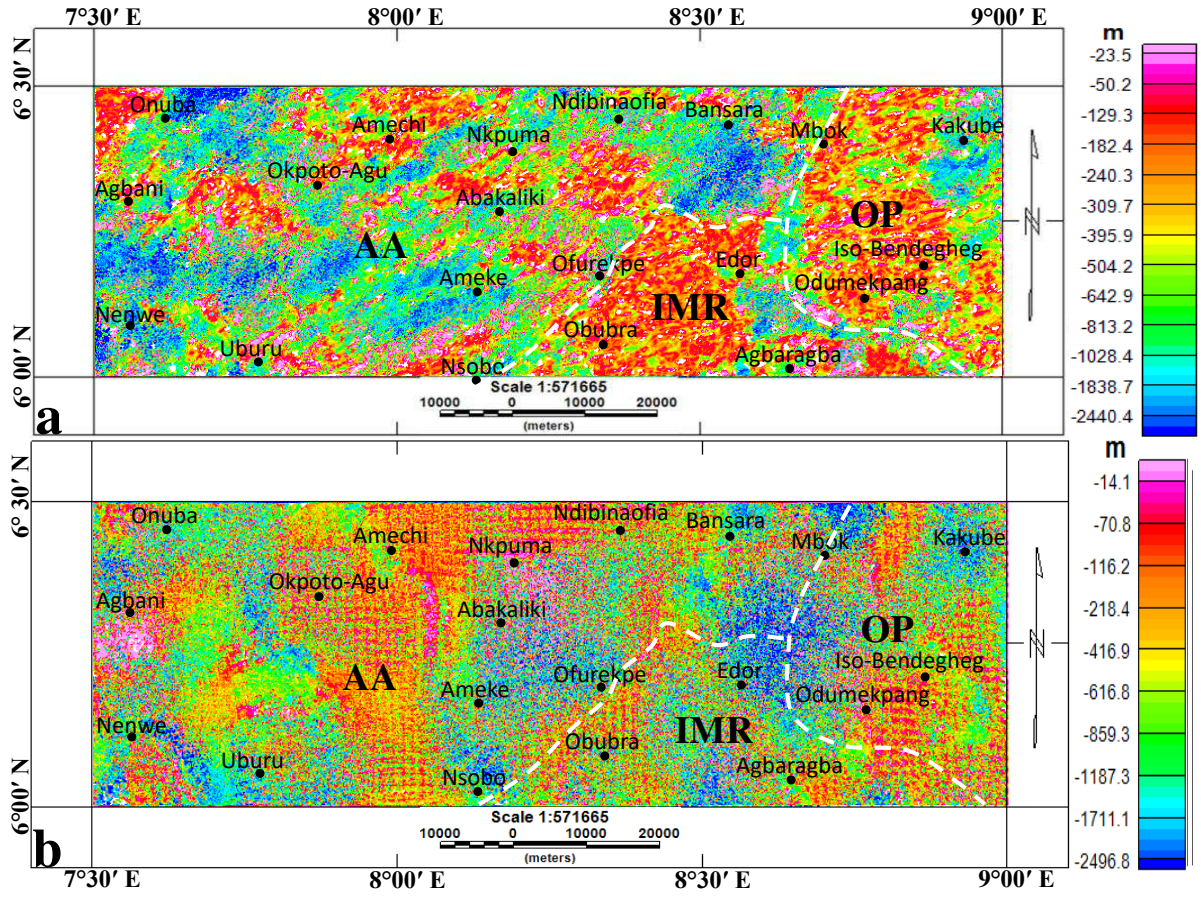

Fig. 9: Euler deconvolution maps of (a) total magnetic intensity and (b) Bouguer gravity data (structural index=1.0; max. % depth tolerance=15.0, window size=10).

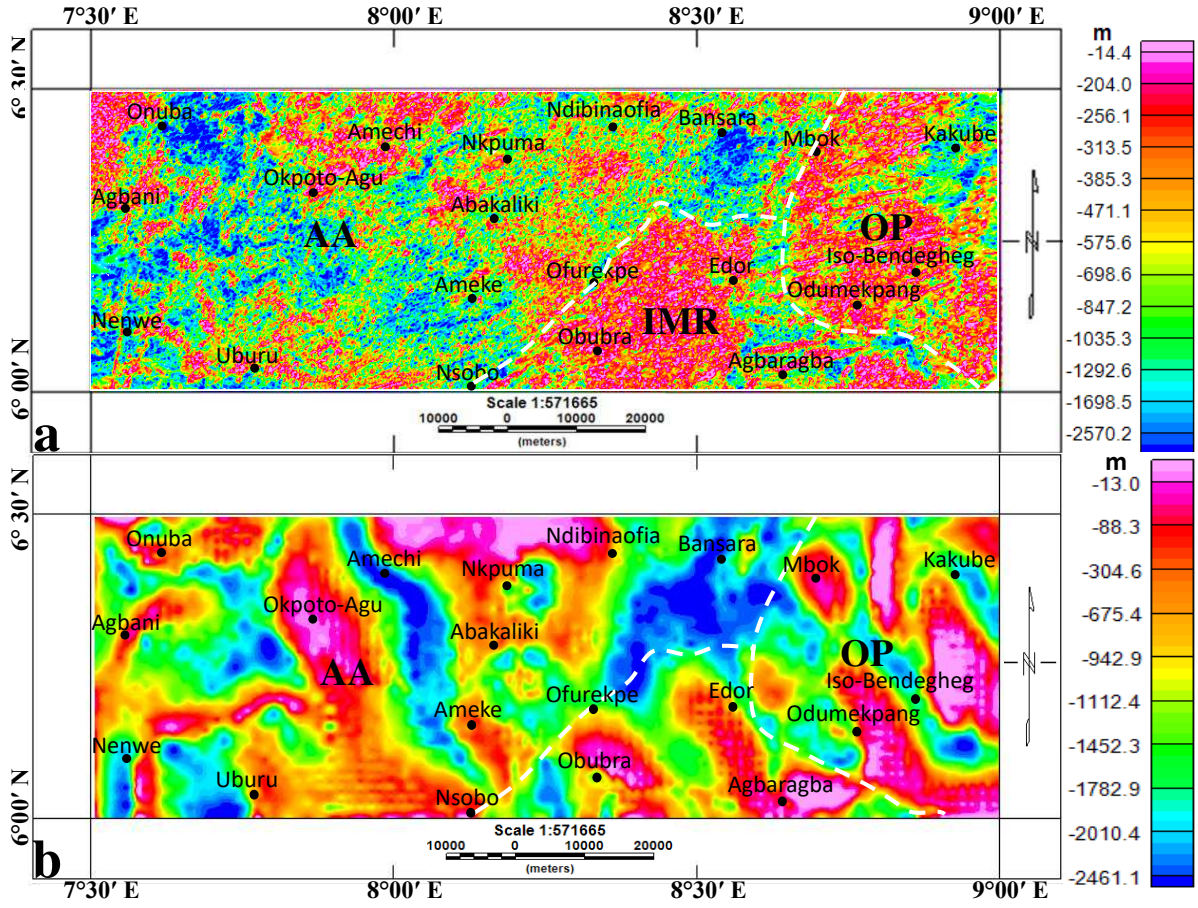

Fig. 10: Source parameter imaging maps of (a) total magnetic intensity and (b) Bouguer gravity data.

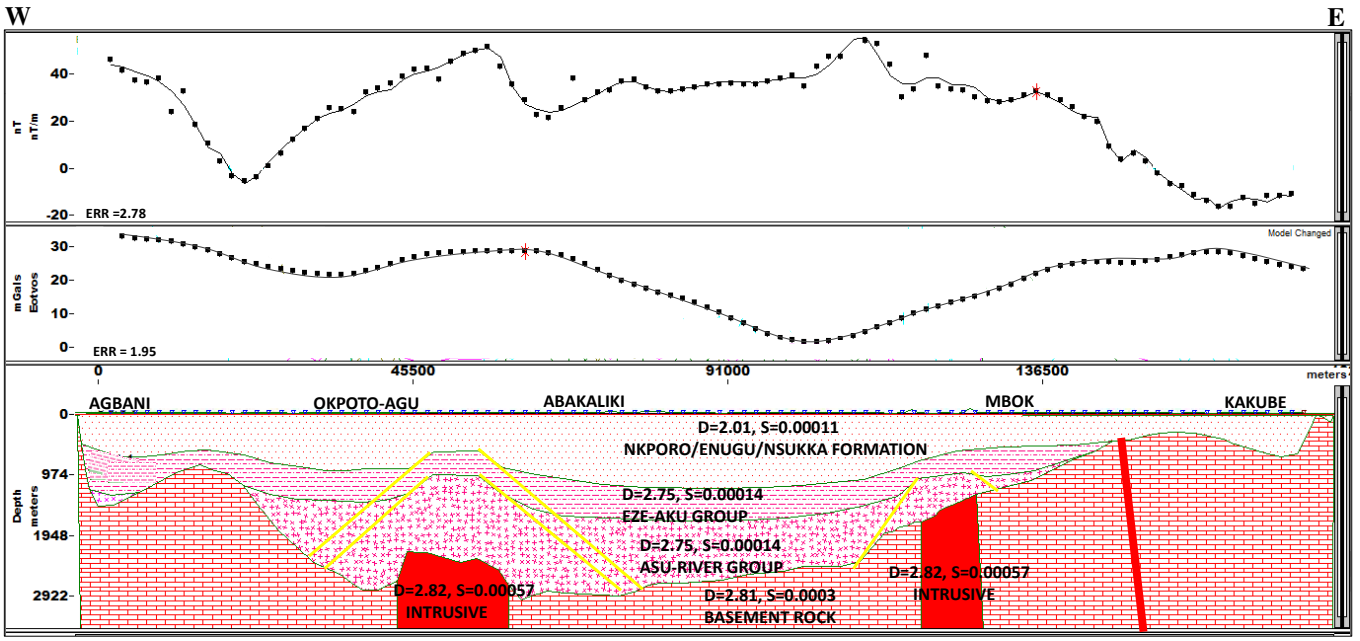

Fig. 11: 2-D joint magnetic and gravity model obtained from profile one.

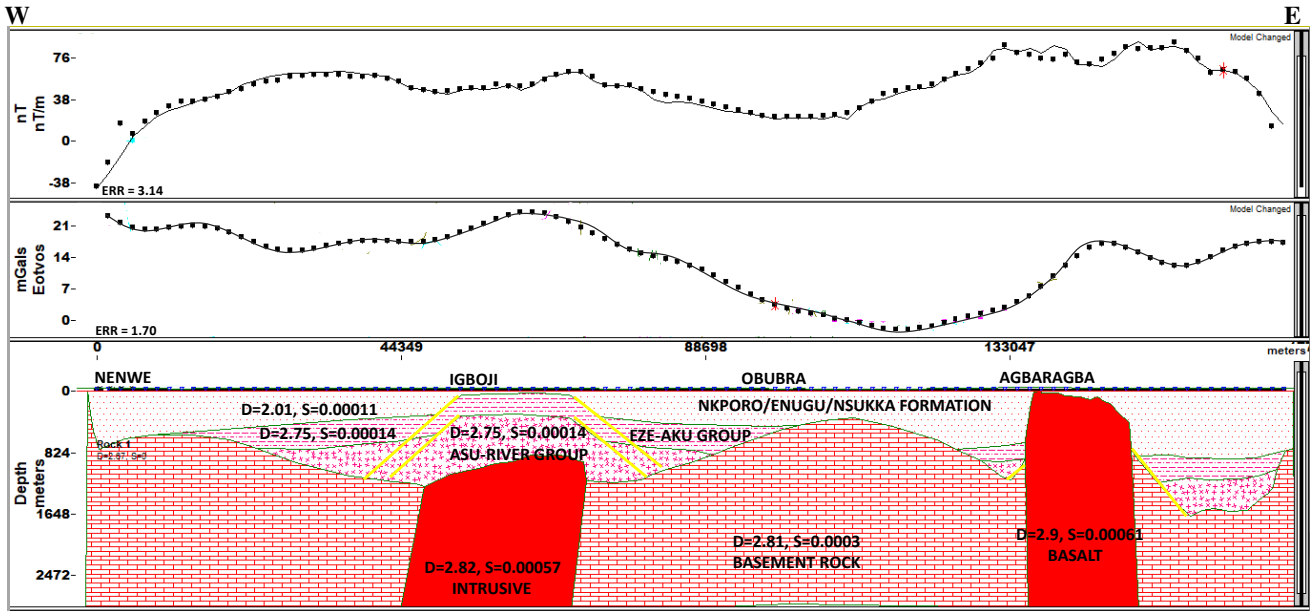

Fig. 12: 2-D joint magnetic and gravity model obtained from profile two.

Figures

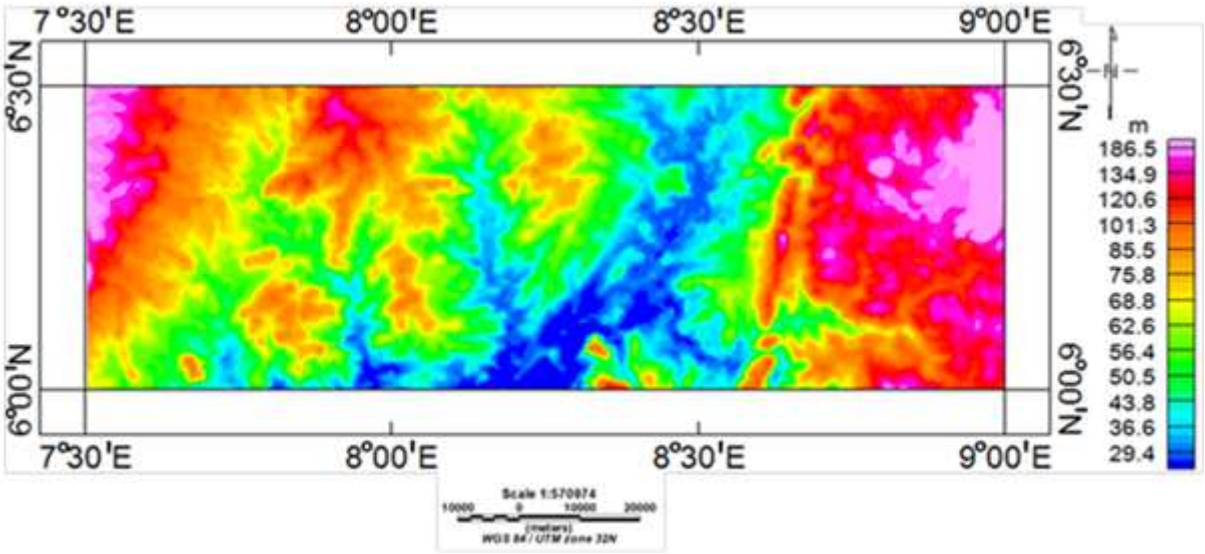

Figure 1

Digital elevation map of the study area. Note: The designations employed and the presentation of the material on this map do not imply the expression of any opinion whatsoever on the part of Research Square concerning the legal status of any country, territory, city or area or of its authorities, or concerning the delimitation of its frontiers or boundaries. This map has been provided by the authors.

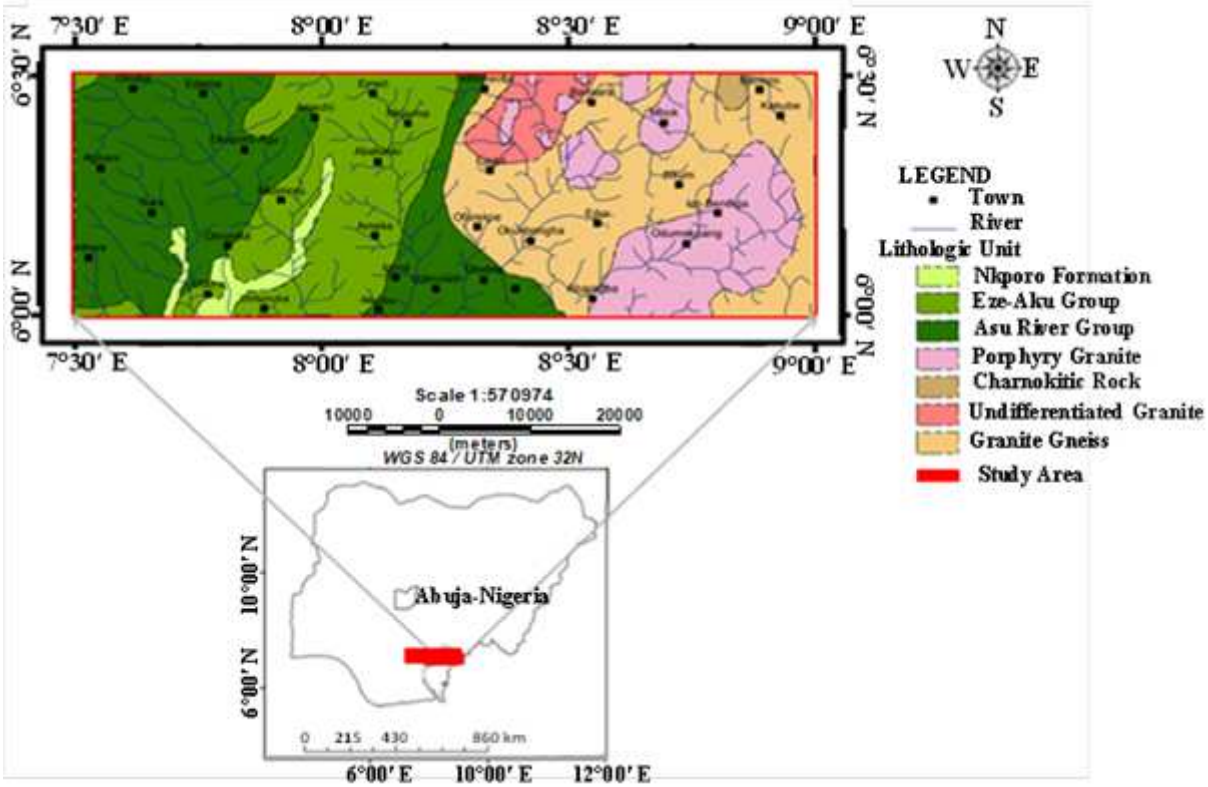

Figure 2

Geologic map of the study area. Note: The designations employed and the presentation of the material on this map do not imply the expression of any opinion whatsoever on the part of Research Square concerning the legal status of any country, territory, city or area or of its authorities, or concerning the delimitation of its frontiers or boundaries. This map has been provided by the authors.

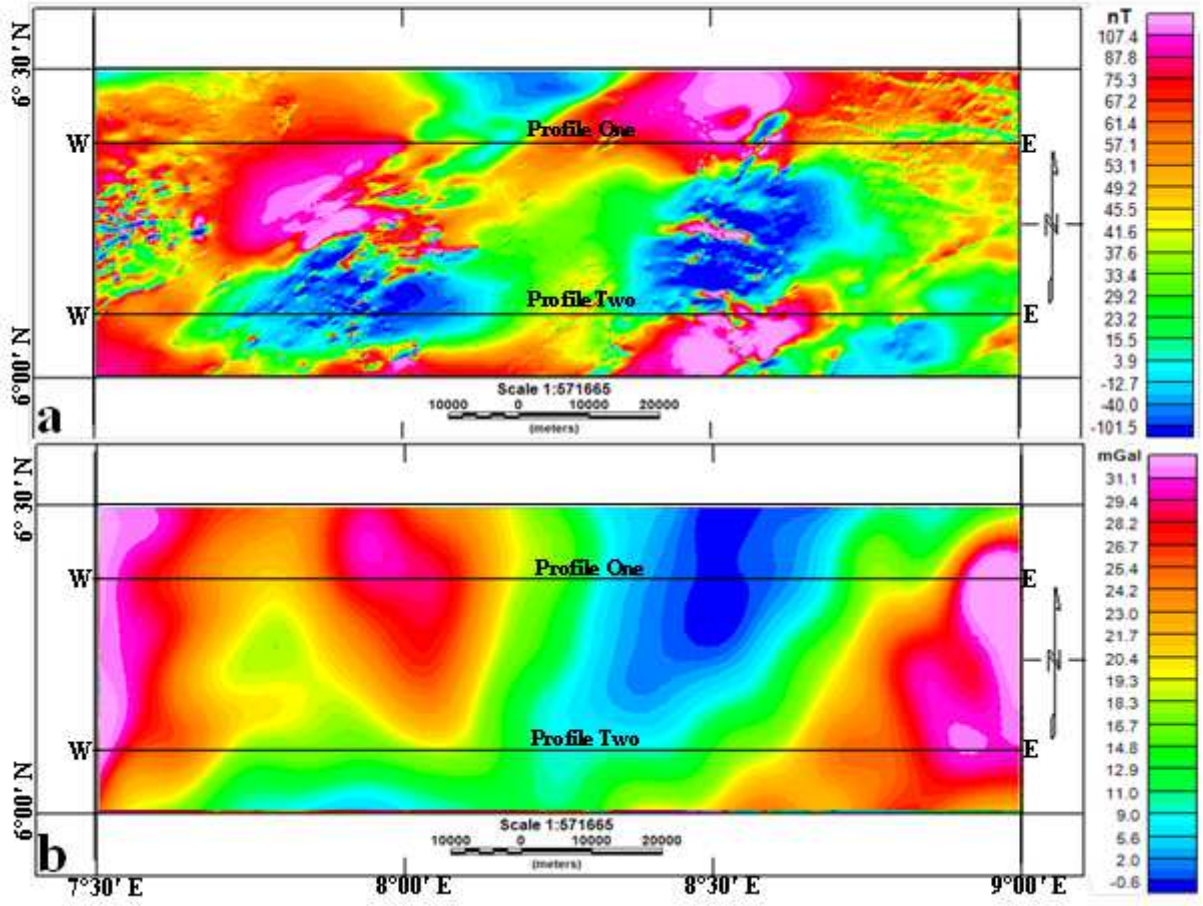

Figure 3

(a) Total magnetic intensity and (b) Bouguer gravity gridded maps. Note: The designations employed and the presentation of the material on this map do not imply the expression of any opinion whatsoever on the part of Research Square concerning the legal status of any country, territory, city or area or of its authorities, or concerning the delimitation of its frontiers or boundaries. This map has been provided by the authors.

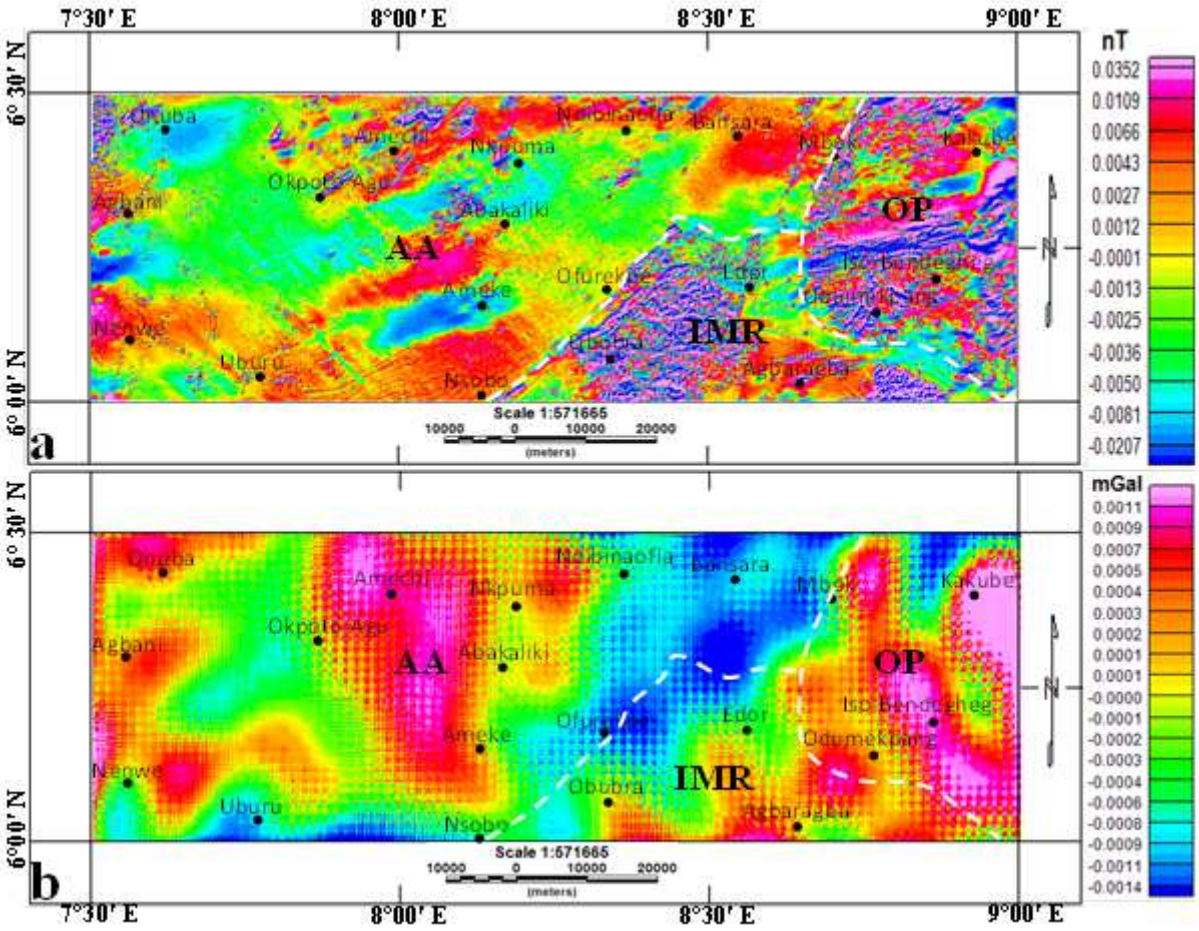

Figure 4

First vertical derivative maps of (a) total magnetic intensity and (b) Bouguer gravity data. Note: The designations employed and the presentation of the material on this map do not imply the expression of any opinion whatsoever on the part of Research Square concerning the legal status of any country, territory, city or area or of its authorities, or concerning the delimitation of its frontiers or boundaries. This map has been provided by the authors.

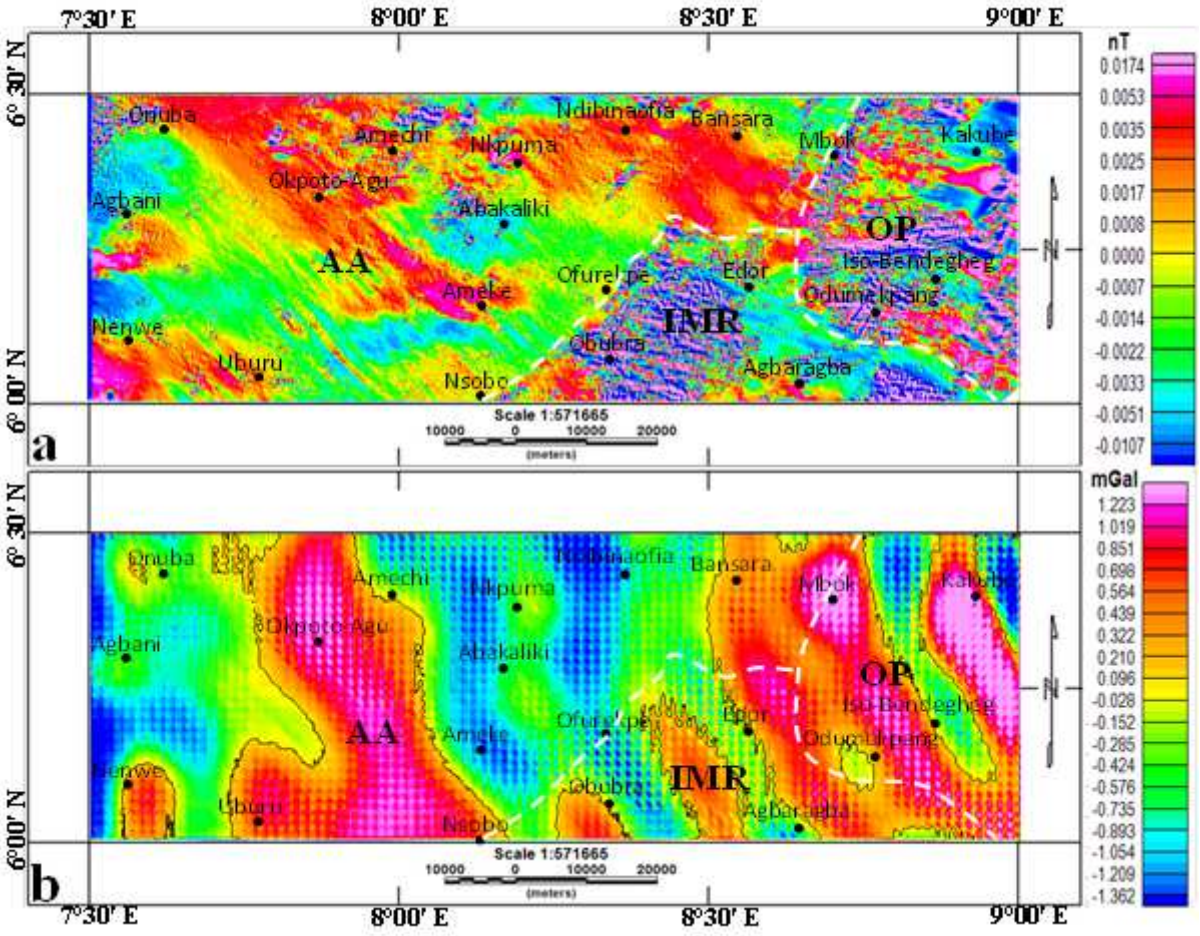

Figure 5

Total horizontal derivative maps of (a) total magnetic intensity and (b) Bouguer gravity data. Note: The designations employed and the presentation of the material on this map do not imply the expression of any opinion whatsoever on the part of Research Square concerning the legal status of any country, territory, city or area or of its authorities, or concerning the delimitation of its frontiers or boundaries. This map has been provided by the authors.

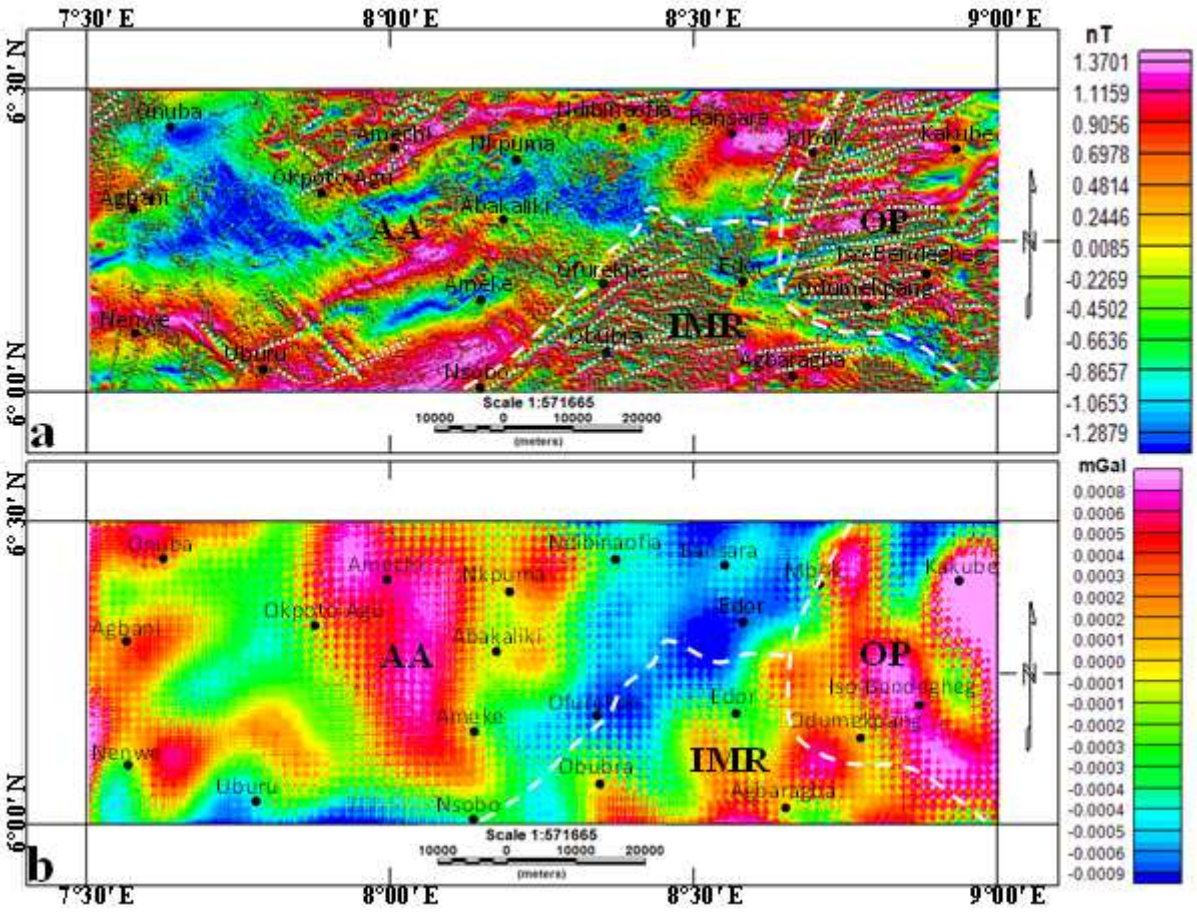

Figure 6

Tilt angle derivative maps of (a) total magnetic intensity and (b) Bouguer gravity data. Note: The designations employed and the presentation of the material on this map do not imply the expression of any opinion whatsoever on the part of Research Square concerning the legal status of any country, territory, city or area or of its authorities, or concerning the delimitation of its frontiers or boundaries. This map has been provided by the authors.

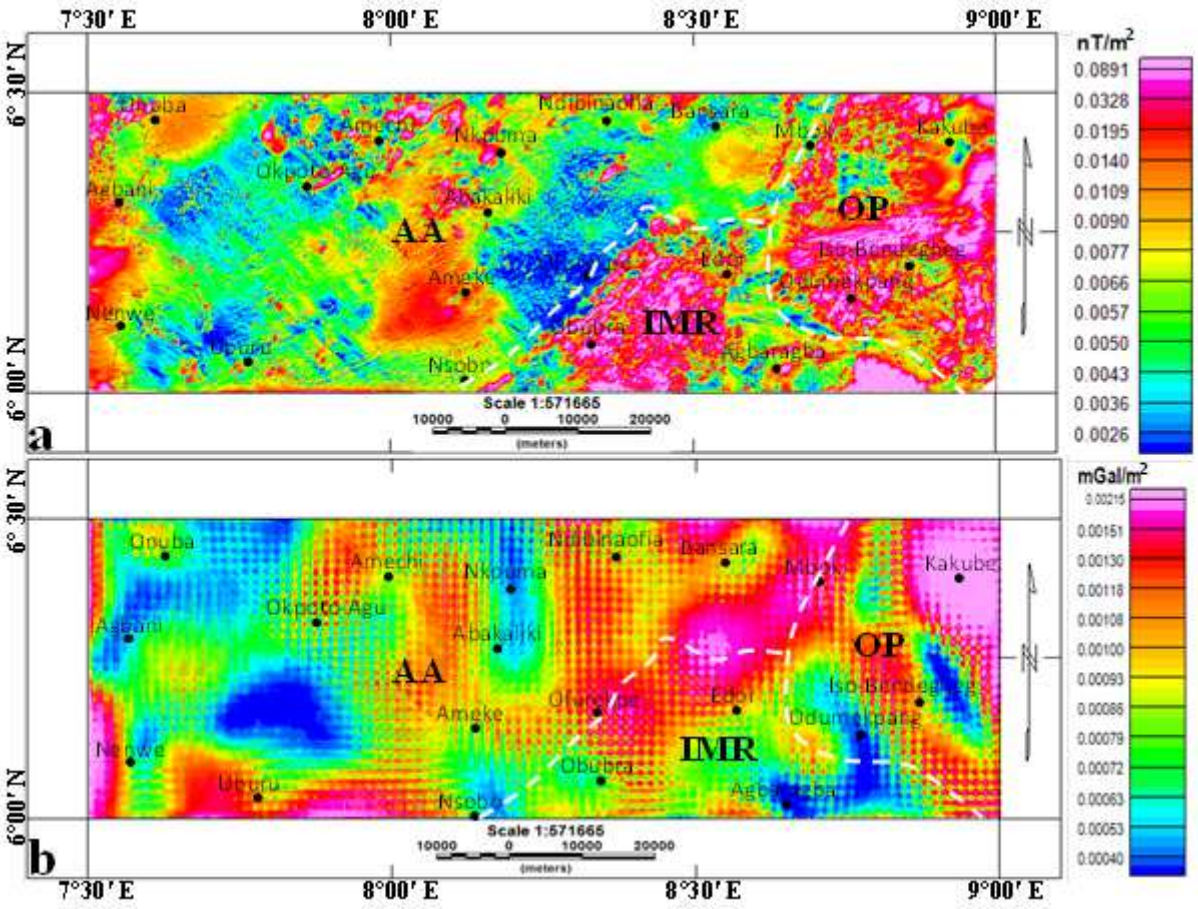

Figure 7

Analytic signal maps of (a) total magnetic intensity and (b) Bouguer gravity data. Note: The designations employed and the presentation of the material on this map do not imply the expression of any opinion whatsoever on the part of Research Square concerning the legal status of any country, territory, city or area or of its authorities, or concerning the delimitation of its frontiers or boundaries. This map has been provided by the authors.

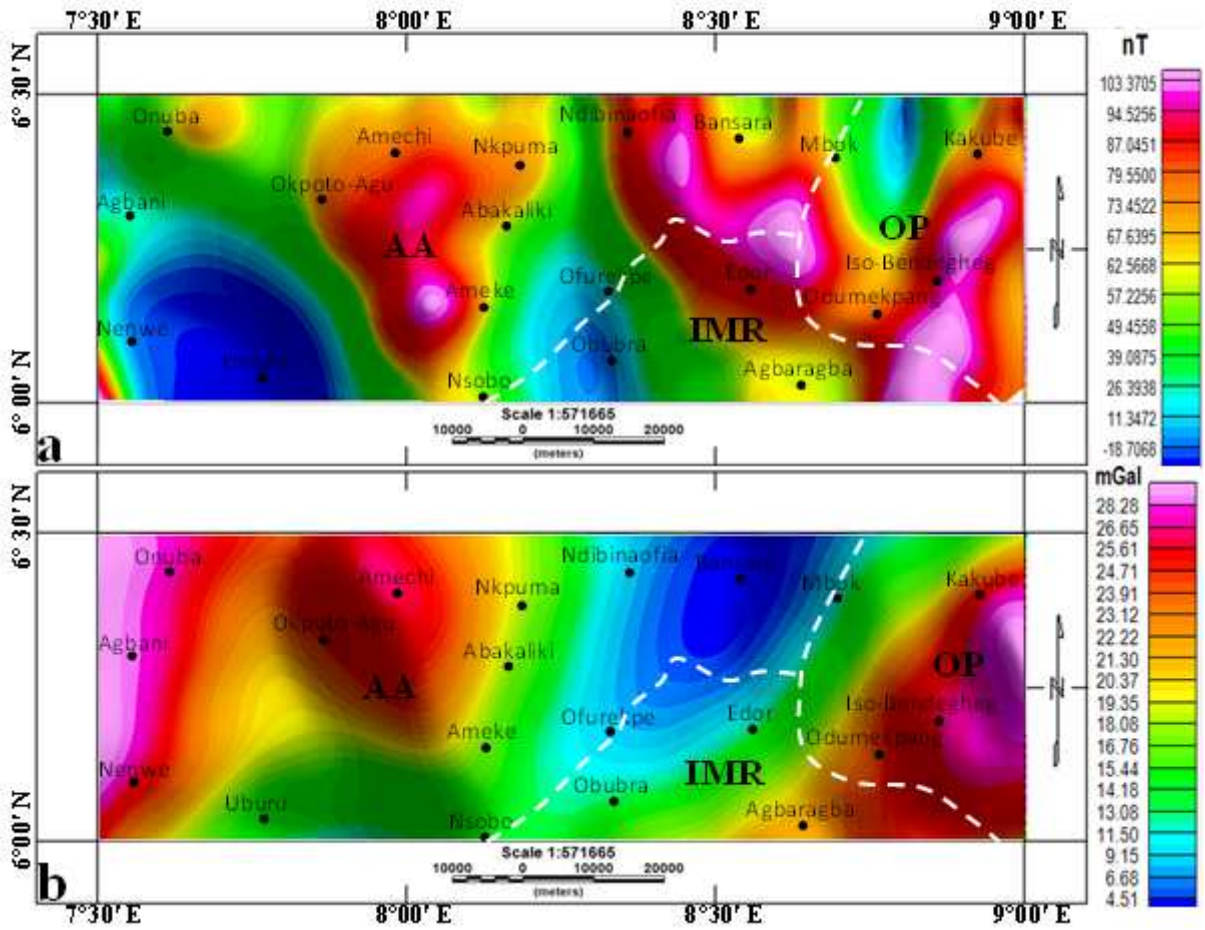

Figure 8

Upward continued to 5000 m maps of (a) total magnetic intensity and (b) Bouguer gravity data. Note: The designations employed and the presentation of the material on this map do not imply the expression of any opinion whatsoever on the part of Research Square concerning the legal status of any country, territory, city or area or of its authorities, or concerning the delimitation of its frontiers or boundaries. This map has been provided by the authors.

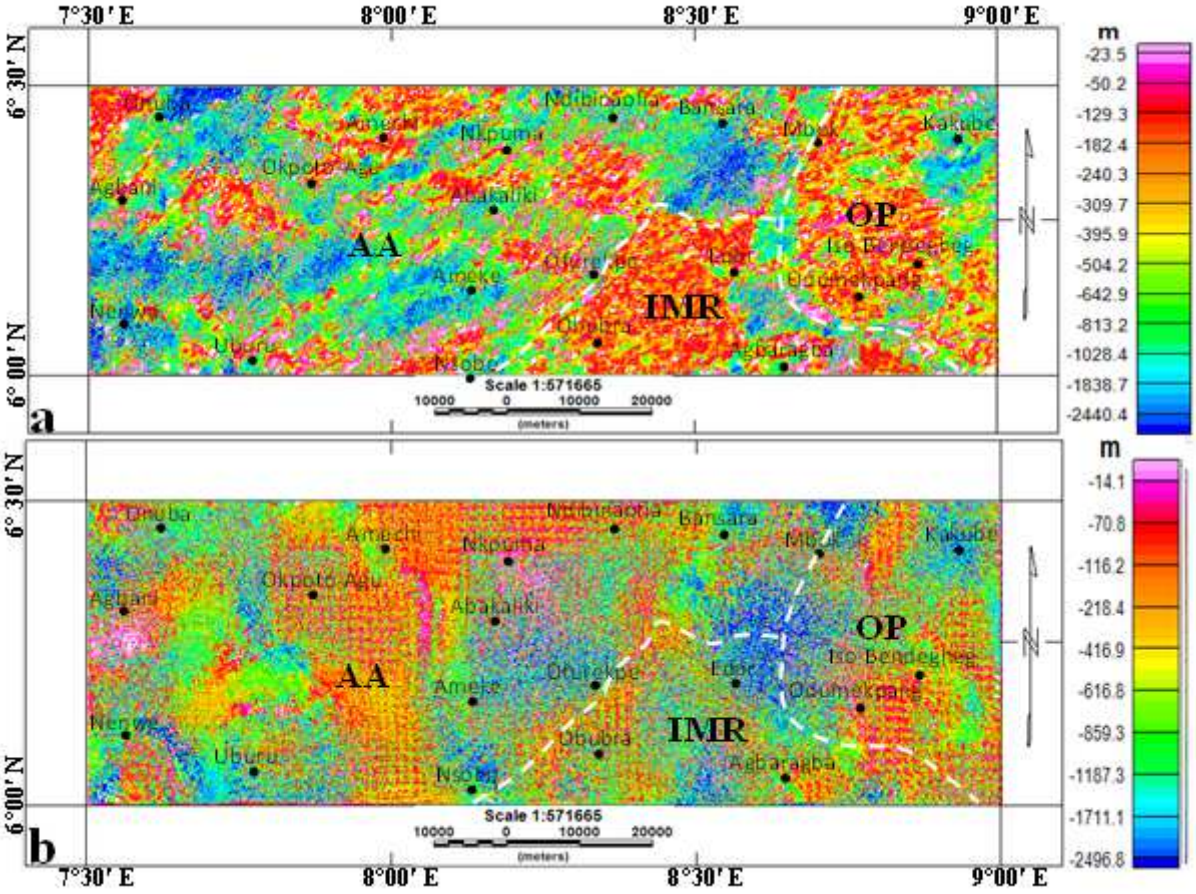

Figure 9

Euler deconvolution maps of (a) total magnetic intensity and (b) Bouguer gravity data (structural index=1.0; max. % depth tolerance=15.0, window size=10). Note: The designations employed and the presentation of the material on this map do not imply the expression of any opinion whatsoever on the part of Research Square concerning the legal status of any country, territory, city or area or of its authorities, or concerning the delimitation of its frontiers or boundaries. This map has been provided by the authors.

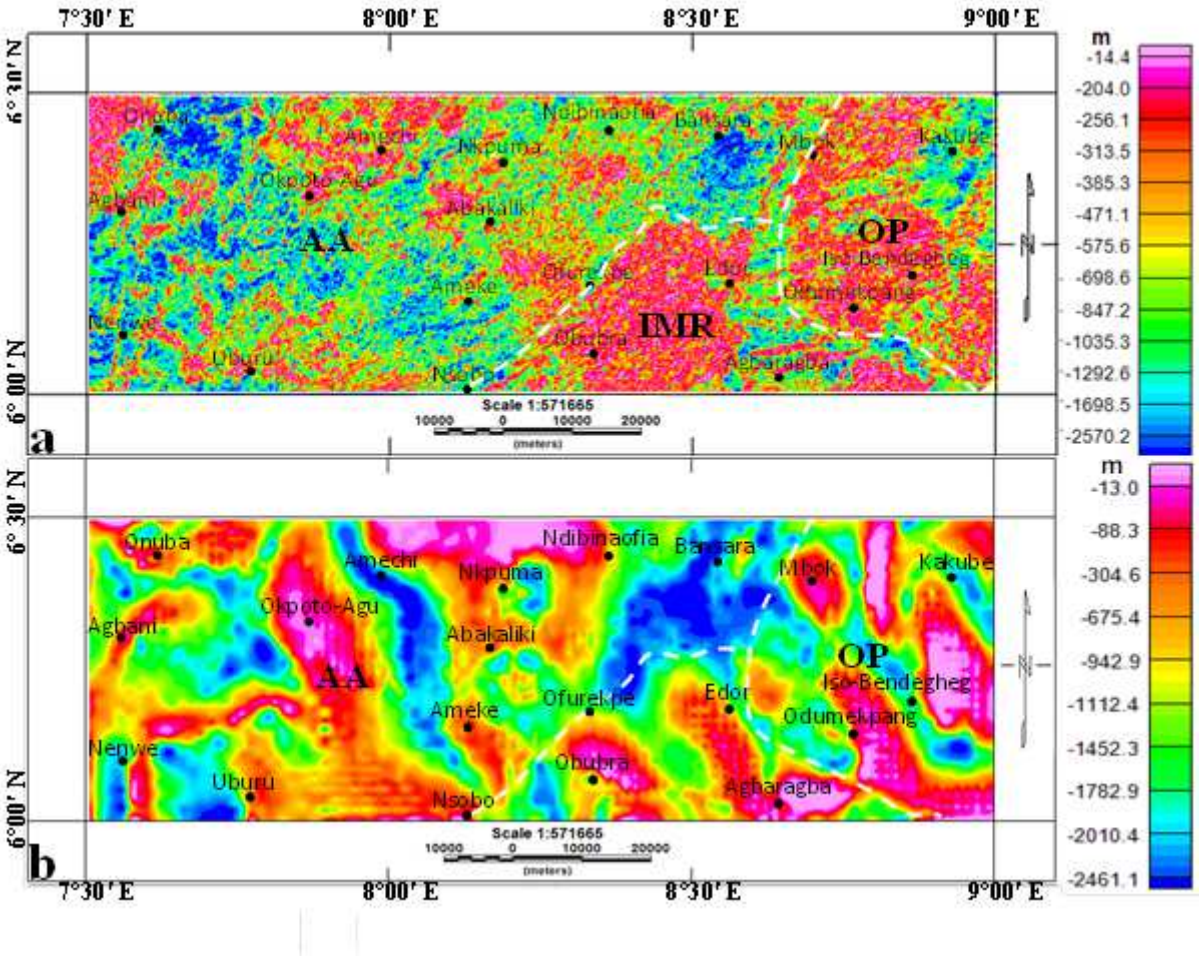

Figure 10

Source parameter imaging maps of (a) total magnetic intensity and (b) Bouguer gravity data. Note: The designations employed and the presentation of the material on this map do not imply the expression of any opinion whatsoever on the part of Research Square concerning the legal status of any country, territory, city or area or of its authorities, or concerning the delimitation of its frontiers or boundaries. This map has been provided by the authors.

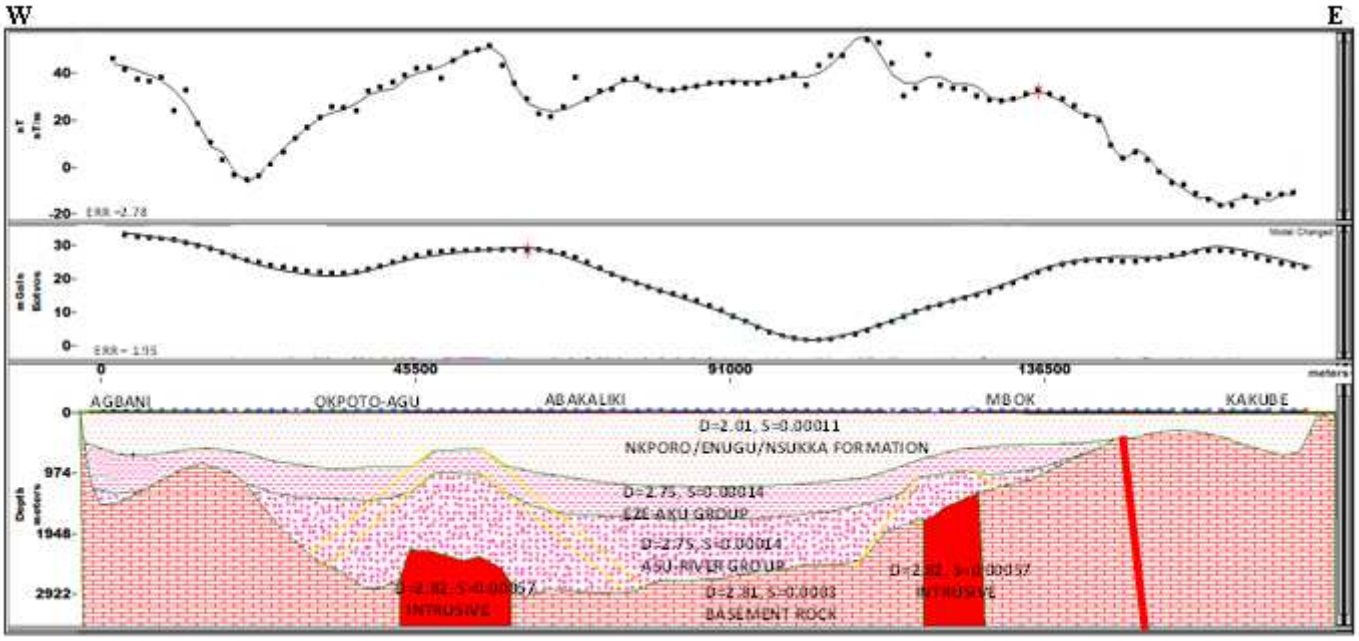

Figure 11

2-D joint magnetic and gravity model obtained from profile one. Note: The designations employed and the presentation of the material on this map do not imply the expression of any opinion whatsoever on the part of Research Square concerning the legal status of any country, territory, city or area or of its authorities, or concerning the delimitation of its frontiers or boundaries. This map has been provided by the authors.

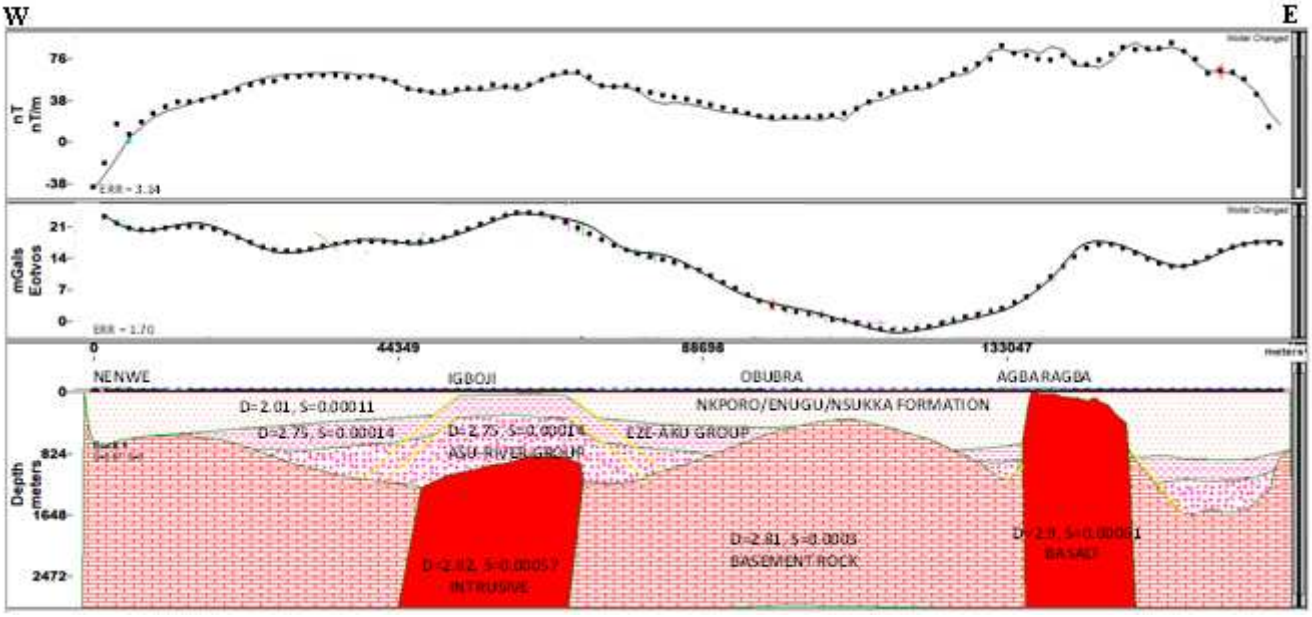

Figure 12

2-D joint magnetic and gravity model obtained from profile two. Note: The designations employed and the presentation of the material on this map do not imply the expression of any opinion whatsoever on the part of Research Square concerning the legal status of any country, territory, city or area or of its

authorities, or concerning the delimitation of its frontiers or boundaries. This map has been provided by the authors.